7-2014

Experimental investigation on the shear characteristics of GFRP reinforcement systems embedded in concrete.

Austin Beau Connor
University of Louisville

EXPERIMENTAL INVESTIGATION ON THE SHEAR CHARACTERISTICS OF GFRP REINFORCEMENT SYSTEMS EMBEDDED IN CONCRETE

By

Austin Beau Connor
B.S., University of Louisville, 2013

A Thesis
Submitted to the Faculty of the
University of Louisville
J. B. Speed School of Engineering
as Partial Fulfillment of the Requirements
for the Professional Degree

MASTER OF ENGINEERING

Department of Civil and Environmental Engineering

July 2014

EXPERIMENTAL INVESTIGATION ON THE SHEAR CHARACTERISTICS OF GFRP REINFORCEMENT SYSTEMS EMBEDDED IN CONCRETE

Submitted By: _____
Austin Beau Connor

A Thesis Approved On

_____
(Date)

by the Following Reading and Examination Committee:

_____
Young Hoon Kim, Thesis Director

_____
William M. McGinley

_____
James E. Lewis

ACKNOWLEDGEMENTS

I wish to express my gratitude to everyone who assisted me in the completion of this project. To my faculty advisor, Dr. Young Hoon Kim, I wish to express my sincerest gratitude and appreciation. I am grateful for the opportunity to work with you on this project and I am grateful for your guidance, support and encouragement throughout this process. Thank you to Dr. Mark McGinley and Dr. James Lewis for serving as my committee members. I would also like to thank Dr. Jeff Kiesel for assisting in the programming of the data acquisition system and the staff and students in the Civil engineering laboratory for assisting with fabrication and testing of test specimens.

The financial support provided by the Intramural Research Incentive Grant (IRIG), Commission on Diversity and Racial Equality (CODRE) and the Multimodal Transportation & Infrastructure Consortium (MTIC) Tier I UTC through the U.S Department of Transportation made this project possible, and I am thankful for the opportunity. I would like to thank Hughes Bros Inc. and CEMEX for donating materials and providing technical support on their products.

Finally, I wish to thank my friends and family for their continuous support and encouragement throughout this process. It would not have been possible without you all.

ABSTRACT

To mitigate the deterioration of steel-reinforced concrete members, a fiber-reinforced polymers (FRPs) system has been introduced and has increasingly been used to replace the conventional steel reinforcing bar. However, questions remain about the performance of the Glass Fiber Reinforced Polymer (GFRP) reinforcing bar in concrete with varied stress orientation and shape. The GFRP reinforcement is an anisotropic material that possesses low strength for the transverse direction. This paper presents the results of the shear performance of GFRP reinforcement crossing varied crack angles. Fifteen push-off specimens were tested to investigate the shear characteristics of the GFRP and steel reinforcement. Tests were performed with three varied orientations of steel and GFRP reinforcement embedded in concrete: 90, 45, and 135-degrees with respect to the shear crack plane. In addition, the group-effect of GFRP reinforcement is also investigated with two reinforcing bars. Results indicate that the contributions of aggregate interlock and GFRP reinforcement are significantly varied depending on the bar orientation. Varied orientation of the GFRP bar across the crack plane allows for different failure modes of the reinforcement and absorbed energy capacities. Maximum shear capacity is obtained in specimen with 135-degree orientation accompanying with minimized crack width. This indicates that 135-degree orientation promoted higher aggregate interlock and sufficient development of strength in the reinforcement.

TABLE OF CONTENTS

LIST OF FIGURES

LIST OF TABLES

I. INTRODUCTION

A. General

America's economic growth, and specifically its ability to compete in the global marketplace, is directly related to the health of the nation's infrastructure including its bridges, roadways and dams. Of particular importance are its bridges, a fundamental link for both millions of daily commuters and commercial freight. Over the last decade, the United States has increased efforts to prioritize the repair and replacement of functionally obsolete and structurally deficient bridges. On average 200 million daily trips are made across structurally deficient bridges located in the 102 largest metropolitan cities in the United States. Further illustrating this point, 66,749, or one-third, of the nation's bridges are classified as structurally deficient (ASCE 2013), and while repair projects are underway, they generally involve bridges that are smaller in scale. In 2009, the Federal Highway Administration (FHWA) estimates that more than 30-percent of existing bridges had exceeded their 50-year design life, concluding that significantly more investment in the coming years, upwards of $76 billion, would be required. Between 2009 and 2013, billions of dollars were spent annually on bridge construction, rehabilitation and repair (FHWA 2013). In spite of this, the average age of the nation's bridges declined by only one year, from an average age of 43 years in 2009 to 42 years in 2013. Therefore, even greater funding levels will be needed to replace the nation's larger and longer urban bridges that carry the highest percentages of daily traffic.

With the cost of repair and rehabilitation being significantly high, it is essential that cost-efficient construction materials and innovative transportation technologies be developed and implemented to help relieve these costs. Recently, composites have become

popular in industry, bringing new development in structural and nonstructural applications. Composites, various types of fiber-reinforced polymers (FRPs), have many advantages over conventional steel reinforcement, exhibiting high tensile strength and stiffness, durability against corrosion, and lower life-cycle costs. An indicator of the increasing popularity of composite reinforcement is reflected in the American Association of State Highway Transportation Officials (AASHTO) recent efforts to encourage the use of composite reinforcement in bridge deck elements (AASHTO 2009). Similarly, the Canadian Highway Bridge Design Code (CSA 2006; CSA 2012) allows the use of FRPs as primary reinforcement and pre-stressing tendons in concrete. As with any new material, extensive research and development is needed to standardize methods for use in design and construction. Hence, potential applications of composite reinforcement for future structural elements will increase in order to minimize cost and reduce the time required to construct bridge elements, while increasing structural integrity and durability. However, challenges remain for structural engineers. The following section will discuss both current and future challenges.

B. Problem Statement

Many studies focus on the utilization of GFRP reinforcement in flexural elements to resist tensile stresses rather than the bar's shear performance. Despite the number of investigations on the mechanical performances of composite reinforced concrete, design methods to utilize composite reinforcement efficiently and safely have not been fully developed. Even though FRP is an anisotropic material, it is more durable and mechanically superior to conventional reinforcing steel. An anisotropic material is not uniform throughout and has different characteristics relating to strength depending on the

direction of applied force. FRPs are weakest in the transverse direction, perpendicular to the fibers. Therefore, its shear characteristics are an important design consideration. However, the brittleness of FRP using current design equations and models leads to an underestimation of its true shear capacity, and the shear characteristics are not fully understood. Therefore, the design tends to be conservative, resulting in excessive usage of GFRP reinforcement. Challenges that limit the use of composite reinforcement include the bond between FRP and concrete, shear strengths of structural elements, long-term performance in concrete, and durability in harsh environmental conditions.

C. Research Significance

Currently, design methods for FRP reinforcement in concrete is based upon that of steel reinforcement, and the design equations are merely adopted from its steel counterpart. Therefore, there is a need for further development to provide a more detailed model to predict its behavior as reinforcement in concrete. In this study, glass fiber reinforced polymer-reinforcement (GFRP) will be used to investigate the shear characteristics embedded in concrete, with the goal of advancing current design methodologies. Achieving these research goals will also have a broader impact on the design of FRP reinforced concrete systems. This study is being conducted to propose accurate and practical design guidelines that provide a more consistent and rational approach, and as a first step, the shear characteristics are investigated in this experimental program.

D. Research Objectives

The major objective of this research is to investigate the shear behavior of GFRP bars embedded in concrete. Push-off specimens will be fabricated using GFRP and steel reinforcing bars and tested to compare behavior. The main variable of the experimental

program is the orientation of reinforcement with respect to the shear plane. Various types of testing will determine the properties of the concrete and reinforcement used.

E. Organization of Thesis

This thesis consists of five chapters. Chapter I outlines the contents of the thesis and an overview of the research conducted. Chapter II contains a literature review on the properties, mechanics, benefits, shortfalls, and applications of FRP materials in construction. Also discussed in this chapter are the variables that affect the shear characteristics FRP bars in concrete. The current design codes and models developed by other researchers will also be discussed. Chapter III describes that materials used during this project and the test matrix of the experimental program. Chapter IV presents the experimental results, and analysis using energy absorption to quantify the contribution of aggregate interlock and reinforcement to shear capacity. Chapter V provides the conclusion, limitations of the study and recommendations for future research.

II. BACKGROUND AND LITERATURE REVIEW

A. Basics of FRP and Applications

FRPs are composite materials composed of high-strength fibers embedded in a polymer matrix or resin. Like many other composites, such as concrete, two materials act in unison, overcoming the deficits of the other. Whereas the resin is strong in compression and relatively weak in tension, fibers are very strong in tension but do not contribute much resistance to compression. The resin is the polymer matrix used to bond together fibers. While the primary function of the resin is to coat and protect the fibers from abrasion or corrosion, it also acts as a transfer mechanism to distribute applied loads to each fiber, making the composite stronger. The matrix also transfers inter-laminar and in-plane shear stresses in the FRP and provides lateral support against buckling when subjected to compressive loads (ACI 440 2006). After extensive research and development, FRPs are beginning to see use in numerous engineering and construction applications. Structures and various elements can be fabricated entirely out of FRP composites such as bridge decks and utility poles as show in FIGURE 1.

FIGURE 1 – FRP Structural Elements: (a) GFRP Bridge Decking (b) FRP Utility Poles

FRP rebar and reinforcing grids have been used successfully as internal reinforcement in concrete beams and slabs (El-Sayed et al. 2005). FRPs are also resistant to de-icing chemicals, low alkali and salts, more durable, and less maintenance intensive, making it a better choice compared to steel for use in roadways and bridge decks (Wegian and Abdalla 2005). FRPs are also ideal for electromagnetically sensitive applications. The material is nonconductive and will not transmit current or interfere with the operation of nearby electronic devices. This provides a safer environment in nuclear power plants, specialized military structures, air traffic control towers, hospitals, and electrical/phone transmission towers (Keller 2001).

The most common composites used in engineering applications are aramid (AFRP), carbon (CFRP) and glass (GFRP) fibers. Each can be manufactured into sheets, plates, and wraps to strengthen existing structures, or as bars, rods and tendons for internal reinforcement in concrete members as shown in FIGURE 2 (Ametrano 2011). FRP has several other added benefits including high specific strength and stiffness, enhanced fatigue life, high strength to weight ratios, noncorrosive, has controlled thermal and electromagnetic properties, and low life-cycle costs.

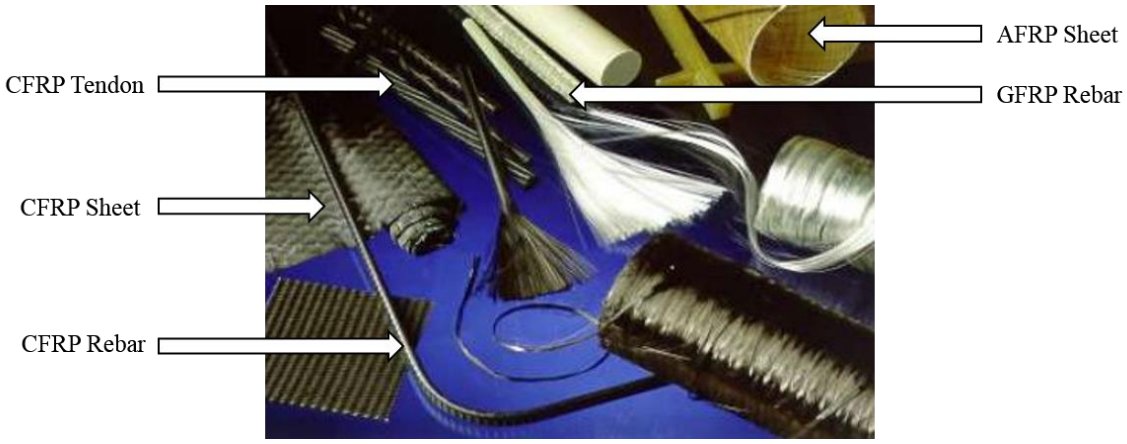

FIGURE 2 – Various FRPs as Reinforcement in Concrete Structures (Ametrano 2011)

For example, FRPs tensile strength is typically 1.5 to 5 times than steel at a given weight, which indicates high specific strength and high strength to weight ratios. A higher strength to weight ratio allows for a greater load carrying capacity, and possibly an overall reduction in the size and weight of the structure. However, while the initial cost of FRP reinforcement is generally higher than standard steel rebar and is comparable to epoxy-coated steel rebar, when considered on a lifecycle cost basis, it is quite economical. Its primary uses are typically in non-prestressed elements subjected to flexural, shear and compressive loading that usually require frequent repair and maintenance. For all these reasons and more, FRP has slowly begun to gain strength in the engineering and construction industries. In this study, the literature review focuses on GFRP reinforcement.

With the advantages of FRP materials previously discussed, there are several disadvantages worth mentioning. While being cost effective, the initial cost of implementing FRPs is significantly higher when compared to conventional steel. The added expense could potentially cause a project to be over budget. In addition, FRPs low modulus of elasticity attributes to a deflection driven design, which does not allow a designer to utilize the full strength of the material. Special consideration is also needed to account for the response to thermal change, as FRP differs from steel. A thorough analysis of the materials behavior requires a finite element model because strength and stiffness of FRP degrades over time. The resulting creep must also be addressed during design and appropriate strength reduction factors should be used to ensure adequate stiffness over the entire service life of the structure (FHWA 2013). Finally, there is a lack in long-term performance data for the use of FRPs in concrete because current systems use proprietary designs and manufacturing methods. For example, high alkali (pH of 13) in concrete

degrades the interface between fiber and resin over time resulting in the reduction of tensile strength and high probability of failure of the GFRP reinforced concrete specimens (Gardoni et al. 2012). However, the disadvantages of FRP materials will decrease as further research and development provides a clear insight of the true behavior of the new material. This will provide the guidelines and appropriate design equations to utilize FRPs to enhance the sustainability of infrastructure systems.

B. Mechanical Properties of FRP

FRPs have different strength properties along each axis, characterized by a high tensile strength along the direction of the reinforcing fibers. This characteristic effects the shear strength and dowel action of FRP bar as well as its bond performance in concrete. GFRP reinforcement's performance embedded in concrete can vary significantly depending on its orientation, shape (e.g. bent and/or straight bar), and exposure conditions. Typically, fibers are wound together in the longitudinal direction and bonded together with a high-strength polymer resin. As shown in FIGURE 3, joining the fibers and resin together in this fashion results in a highly anisotropic material with high and low strength in the longitudinal and transverse directions, respectively.

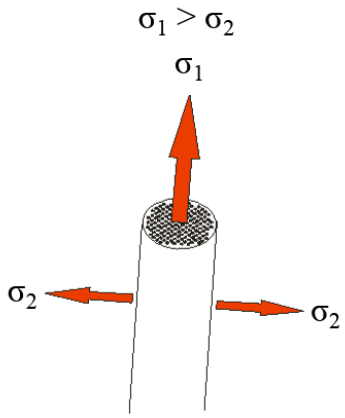

FIGURE 3 – Anisotropic Characteristics of FRPs

In addition, the mechanical properties of FRP vary significantly by the proportions of fibers and resin matrix, and the manufacturing method. All FRPs exhibit linear-elastic tensile stress-strain behavior in the direction of the fibers with no yielding and abrupt failure, in contrast to its steel counterpart. With FRPs being more effective under tension, they are generally used as tensile reinforcement in concrete structures. As shown in TABLE I, GFRP is among the most popular and cost effective material when compared to carbon fiber reinforcement. Generally, GFRP is cheaper than AFRP. Most FRPs also have a lower elastic modulus than steel, excluding some CFRP systems.

TABLE I

TENSILE PROPERTIES OF VARIOUS REINFORCEMENTS (ACI 440 2006)

	Steel	GFRP	CFRP	AFRP
Nominal Yield Stress (ksi)	40 to 75	-	-	-
Tensile Strength (ksi)	70 to 100	70 to 230	87 to 535	250 to 368
Elastic Modulus, $x10^3$ (ksi)	29.0	5.1 to 7.4	16.0 to 84.0	6.0 to 18.2
Yield Strain (%)	0.14 to 0.25	-	-	-
Rupture Strain (%)	6.0 to 12.0	1.2 to 3.1	0.5 to 1.7	1.9 to 4.4
Cost/ft ($)	0.21 to 2.13	0.37 to 6.50	4.45 to 9.10	unknown

Note: "-"is not applicable. (Cost Source: Aslan FRP Sales)

As shown in FIGURE 4, the stress-strain relationship of FRP systems depends on the failure strains of its fibers and resin matrix. Unlike conventional steel reinforcement, FRPs stress-strain relationship has only been modeled up to 0.4 percent of the total tensile strain, and current design is only applicable up to this point (ACI 440 2006). This limitation in the current design process causes excessive material usage and an increase in project costs.

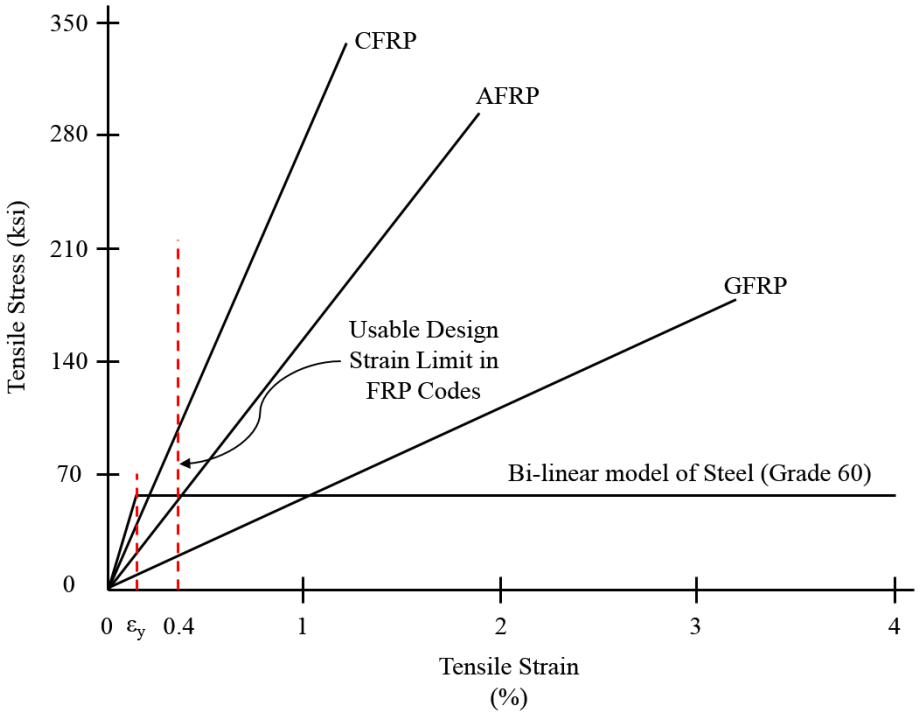

FIGURE 4 – Stress-Strain Response of FRPs Compared to Steel (ACI 440)

Focusing on the properties of GFRP, glass fibers are typically produced using the direct melt process. The fibers are drawn from a glass melt with average diameters ranging from 3 to 25 microns. Glass fibers are generally long and slender, causing high aspect ratios (Ametrano 2011). Of the various typed of glass fibers commercially available, E-glass is the most popular for GFRP composites due to its physical properties and lower cost, as described previously.

C. Shear Mechanisms and Design of GFRP Reinforced Concrete

Typically, in reinforced members, the shear capacity (V_n) is generally the sum of the shear contribution from concrete (V_c) and shear reinforcement (V_s). The need to understand the failure mechanisms is important for composite reinforced structures to quantify each elements contribution to the overall shear capacity of the system. The following sections will explain the shear mechanisms of concrete and the contribution of FRP reinforcement to shear capacity.

1. Shear Mechanisms: Concrete Contribution

The contribution of concrete in an element's total shear capacity is also referred to as the shear friction between cracked surfaces, V_c. The term shear friction was first proposed to define the frictional resistance of cracks to sliding (Birkeland and Birkeland 1966; Mast 1968). Under initially cracked conditions, the sliding plane surfaces are idealized as rough and irregular. These aggregate particles then force the sliding planes apart, and separation induces normal stresses (σ) in the reinforcement crossing the sliding planes, restricting the opening of the sliding planes as shown in FIGURE 5 (Wight and MacGregor 2012). Under high levels of confinement, the sliding planes provide shear resistance and stresses are transferred across the crack face through aggregate interlock.

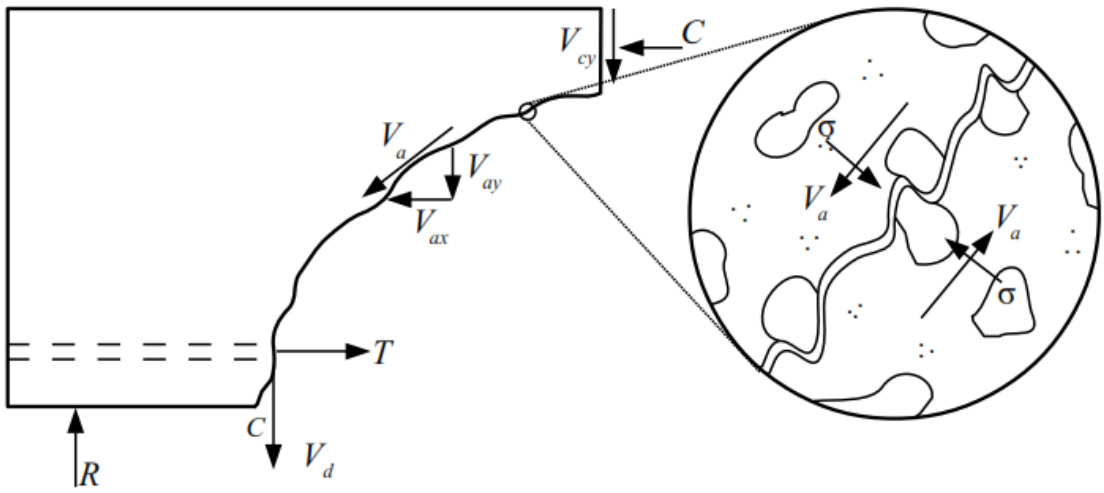

FIGURE 5 – Detail of Aggregate Interlock (Wight and MacGregor 2012)

Shear friction across sliding planes in concrete is a well-established area of current research (Ali et al. 2008; Mansur et al. 2008; Martín-Pérez and Pantazopoulou 2001; Rahal 2010 ; Santos et al. 2010). Two separate shear-friction approaches have been developed previously. Walraven (1981) quantified the shear and normal stress transfer for a range of displacements and separations, now known as the *Walraven Approach*. The *Mattock Approach* quantified the maximum shear stress that could be transferred across cracked and uncracked sections for a range of normal stresses and confinements (Mattock 1974). While flexural mechanisms have been extensively researched, there is not a consensus among engineers and scientists about how to predict the shear strength of FRP reinforced concrete structures during the design process. The basis for determining the contribution of concrete to the overall shear capacity of a reinforced concrete has been thoroughly investigated by numerous researchers (El-Sayed et al. 2005; Tureyen and Frosh 2003).

2. Shear Mechanisms: Reinforcement Contribution

Shear failure of concrete structures with either composite or steel reinforcement is sudden and brittle. For safe design practices, standards provide methods for shear design

of FRP reinforced concrete members. These include, the American Association of Highway Transportation Officials (AASHTO) standard for LRFD Bridge Design (AASHTO 2009), American Concrete Institute (ACI) standard ACI 440.1R-06 (ACI 440 2006), Canadian Standards Association (CSA) standards CSA S6-06 (CSA 2006), the unpublished CSA S6-09 Addendum and CSA S806-12 (CSA 2012), Japan Society of Civil Engineering (JSCE) standard (JSCE 1997), and the Italian Research Council CNR DT-203/2006 (CNR 2006). In addition, models from other researchers include Hoult et al. (2008), Kara (2011), and Alam and Hussein (2012). However, these methods differ from one another in substance and in how shear contributions are calculated. Furthermore, some of the methods are conservative, while others yield unconservative results (Razaqpur and Spadea 2014). Research about quantifying V_s is relatively limited, hence the need to investigate and quantify V_s of FRP-reinforced concrete members. The following sections summarize the most relevant and recent existing shear design equations for FRP reinforced elements, and definitions for the notation used can be found in Appendix 1.

3. ACI 440.1R-06

The AASHTO code is identical to ACI 440 design method. According to ACI 318 (2011), the nominal shear capacity of a reinforced concrete cross section is the sum of the shear resistance provided by concrete and the steel shear reinforcement. When compared to a steel reinforced section with equal areas of longitudinal reinforcement, a cross section using FRP flexural reinforcement after cracking has a smaller depth to the neutral axis due to a lower axial stiffness. The compression region of the cross section is reduced, resulting in wider crack widths, and lower contributions to shear friction by aggregate interlock. In

addition, due to lower strength and stiffness in the transverse direction, it is assumed that the reinforcement contribution is less than that of an equivalent steel area (ACI 440 2006).

The shear capacity provided by concrete with FRP as the primary reinforcement can be calculated using Equation (1):

$$V_c = 5\sqrt{f'_c}\, b_w c \tag{1}$$

where f'_c is the compressive strength of concrete (psi), b_w is the width of the web (in.), and c is the cracked transformed section neutral axis depth (in.).

For singly reinforced, rectangular cross sections, the neutral axis depth c may be computed as:

$$c = kd \tag{2}$$

$$k = \sqrt{2n_f\rho_f + (n_f\rho_f)^2} - n_f\rho_f \tag{3}$$

$$\rho_f = \frac{A_f}{b_w d} \tag{4}$$

$$n_f = \frac{E_f}{E_c} \tag{5}$$

where k is the ratio of the neutral axis depth to reinforcement depth, d is the distance from extreme compression fiber to centroid of tensile reinforcement (in.), n_f is the modular ratio,

ρ_f is the FRP reinforcement ratio, A_f is the area of shear reinforcement (in.^{2}), E_f is the modulus of elasticity of GFRP reinforcement (psi), and E_c is the modulus of elasticity of concrete (psi).

This formula accounts for the axial stiffness of the FRP reinforcement through the neutral axis and has been shown to provide a reasonable factor of safety for FRP–reinforced specimens across the range of reinforcement ratios and concrete strengths tested to date (Tureyen and Frosh 2003).

According to ACI 318 (2011), the method used to calculate the shear contribution of steel stirrups is applicable when using FRP as shear reinforcement. The shear resistance provided by FRP stirrups perpendicular to the axis of the member V_f can be determined using Equation (6).

$$V_f = \frac{A_{fv} f_{fv} d}{s} \tag{6}$$

where A_{fv} is the amount of FRP shear reinforcement within spacing s (in.^{2}), f_{fv} is the tensile strength of FRP for shear design, taken as the smallest of design tensile strength, f_{fu}, strength of bent portion of FRP stirrups f_{fb}, or stress corresponding to $0.004E_f$ (psi), d is the distance from extreme compression fiber to centroid of tensile reinforcement (in.), and s is the spacing of shear reinforcement (in.).

The stress level in the FRP shear reinforcement should be limited to control shear crack widths and maintain shear integrity of the concrete and to avoid failure of the bent portion of the FRP stirrup. Equation (7) and (8) gives the stress level of FRP shear reinforcement at ultimate for use in design.

$$f_{fv} = 0.004E_f \leq f_{fb} \tag{7}$$

$$f_{fb} = \left(0.05\frac{r_b}{d_b} + 0.3 \right) f_{fd} \leq f_{fd} \tag{8}$$

4. CSA S6-06, S6-09 and S806-12

Vecchio and Collins (1986) defined the original form of the modified compression field theory (MCFT) by testing 30 reinforced concrete panels subjected to uniform strain states in a custom-built testing apparatus. The MCFT was developed by observing the response of a large number of reinforced concrete elements loaded in pure shear and in shear combined with axial stress. Even though tests were more difficult to perform, the experimental results clearly illustrated the fundamental behavior of reinforced concrete in shear. The MCFT aimed to predict the relationships between the axial and shear stresses applied to a membrane element and the resulting axial and shear strains. If the theory can accurately predict the behavior of such an element successfully, it can also be as the basis for various analytical models (Bentz et al. 2006). The most accurate, but most complex, of these models involves representing the structure as an array of biaxial elements and then conducting a nonlinear finite element analysis using computer programs.

To predict the shear strength of concrete members reinforced with FRP reinforcing elements, the following equations from the CSA S6-06 shear provisions can be used. Equations (9) to (13) quantifies the concrete's contribution to the overall shear capacity:

$$V_c = 2.5\beta\varphi_c f_{cr} b_w d_v \sqrt{\frac{E_{fl}}{E_s}} \tag{9}$$

$$\begin{aligned} f_{cr} &= 0.4\sqrt{f_c'} \\ d_v &\geq \begin{cases} 0.9d \\ 0.72h \end{cases} \\ \varphi_c &= 0.75 \end{aligned} \tag{10}$$

$$\beta = \frac{0.4}{1+1500\varepsilon_x}\frac{1300}{1000+s_{ze}} \tag{11}$$

$$\varepsilon_x = \frac{\left(\left(\frac{M_f}{d}\right)+V_f+0.5N_f\right)}{2(E_s A_s)} \leq 0.003 \tag{12}$$

$$A_{v,\min} = \frac{0.3\sqrt{f_c'}bs}{f_{fv}}$$

If $A_v > A_{v,min}, s_{ze} =$ 300 mm,
or if $A_v < A_{v,min}, s_{ze} = 35s_z/(15 + a_g) > 0.85s_z$,
where s_z is the crack spacing parameter and shall be taken as d_v or as the distance between layers of distributed longitudinal reinforcement where each intermediate layer of such reinforcement has an area at least equal to $0.003bs_z$ (13)

Similarly, the contribution provided by the transverse reinforcement can be calculated using the following equations.

$$V_{fv} = \frac{\varphi_f A_{fv} \sigma_{fv} d_v \cot\theta}{s} \tag{14}$$

$$\varphi_f = \begin{cases} 0.5 \text{ for GFRP} \\ 0.75 \text{ for CFRP} \end{cases}$$

$$\sigma_{fv} \text{ is the smaller of } \begin{cases} \left(\frac{\left(0.05 \frac{r_b}{d_b} + 0.3\right) f_{\text{fv}}}{1.5} \right) \\ E_{fv} \varepsilon_{fv} \end{cases} \tag{15}$$

$$\varepsilon_{fv} = 0.0001 \left[f_c^{'} \times \frac{\rho_f E_{fl}}{\rho_{fv} E_{fv}} \right]^{0.5} \times \left[1 + 2 \left(\frac{\sigma_N}{f_c^{'}} \right) \right] \leq 0.0025$$

The CSA S6-09 Addendum of the CSA S6-06 standard greatly improved the CSA formulation and became more accurate. The use of the MCFT for developing the CSA S6 code considers the different modulus of elasticity of FRP reinforcement, and E_{fl} of FRP longitudinal reinforcement was already considered in the strain calculation. This improvement was due to the removal of the strain approach from the CSA S6-06 concrete shear equation by removing the double consideration of the lower E_{fl} with FRP reinforcement compared to steel as shown in Equation (16):

$$V_c = 2.5 \beta \varphi_c f_{cr} b_w d_v \tag{16}$$

The following equations are used to determine the shear strength provided by the transverse reinforcement.

$$V_{FRP} = \frac{\varphi_f A_{fv} \sigma_{fv} d_v \cot\theta}{s} \tag{17}$$

$$\theta = (29 + 7000\varepsilon_x)\left(0.88 + \frac{s_{ze}}{2500}\right) \tag{18}$$

$$\sigma_{fv} \text{ is the smaller of } \begin{cases} \left(\frac{\left(0.05\frac{r_b}{d_b} + 0.3\right) f_{\text{fv}}}{1.5}\right) \\ 0.004E_{fv} \end{cases} \tag{19}$$

$$\varphi_f = \begin{cases} 0.5 \text{ for GFRP} \\ 0.75 \text{ for CFRP} \end{cases} \tag{20}$$

The new edition of CSA S806 (2012) was recently published with additions to reflect the latest research findings. In particular, the new edition introduces new provisions for the use of FRP as confining and longitudinal tension reinforcement in columns and in the design of reinforced and prestressed concrete members against combined moment, shear and torsion and the retrofit of building structures for enhanced ductility and seismic resistance. The nominal shear resistance, V_r, of FRP-reinforced concrete members can be computed as:

$$V_r = V_c + V_{sF} \leq 0.22 f_c' b_w d_v \tag{21}$$

where for sections not having an effective depth exceeding 300 mm and with no axial load acting on them, V_c is calculated as follows:

$$0.2\sqrt{f_c'}b_w d_v \geq V_c = 0.05\lambda\phi_c k_m k_r \sqrt[3]{f_c'}b_w d_v \geq 0.11\sqrt{f_c'}, \quad \text{where } f_c' \leq 60 \text{ MPa} \tag{22}$$

where λ is the concrete density factor and is 1.0 for normal density concrete, ϕ_c is the material resistance factor, k_m and k_r are factors accounting for effect the moment to shear ratio and longitudinal reinforcement rigidity, respectively, on the shear strength of the section under consideration and are given as:

$$k_m = \sqrt{\frac{V_f d}{M_f}} \tag{23}$$

$$k_r = 1 + \sqrt[3]{E_{Fl}\rho_{Fl}} \tag{24}$$

where ρ_{Fl} is the longitudinal reinforcement ratio.

For members with *a/d*, or more generally $M_f/V_f d$, less than 2.5, for value of V_c shall be multiplied by the factor k_a to account for shear resistance enhancement by arch effect (Park and Paulay 1975).

$$1.0 \leq k_a = \frac{2.5V_f d}{M_f} \leq 2.5 \tag{25}$$

To account for size effect in members with an effective depth greater than 300 mm and with less transverse shear reinforcement , the following equation is used.

$$A_{v,\min} = 0.07\sqrt{f_c'}\,\frac{b_w s}{0.4 f_{Fu}} \tag{26}$$

V_c is reduced by multiplying it by the factor k_s where d is in mm.

$$k_s = \left(\frac{750}{450 + d}\right) \le 1.0 \tag{27}$$

The parameters k_m, k_r, k_a, and k_s in the expression for V_c are derived semi-empirically which are supported by mechanics-based rational arguments, but the specific mathematical form of each parameter is calibrated using experimental data (Razaqpur et al. 2011). The parameters reflect the effects of well-known factors on V_c, factors that are described in detail by ACI Committee 445 on Shear and Torsion (1998).

For members with FRP transverse reinforcement perpendicular to the member axis, the contribution of FRP to shear, V_{sF}, is calculated by the following equations:

$$V_{sF} = \frac{A_v f_v d_v}{s}\cot\theta \tag{28}$$

$$\theta = 30 + 7000\varepsilon_1 \tag{29}$$

$$\varepsilon_1 = \frac{\frac{M_f}{d_v} + V_f + 0.5N_f}{2E_F A_F} \tag{30}$$

where ε_1 is given by Equation (30) and the average maximum stress in stirrups crossing diagonal shear cracks, f_v, is taken as the smaller of $0.005E_f$, $0.4f_{Fu}$, or 1200 MPa. In addition,

s is limited to $0.9\cot\theta$ in order to consider the influence of the inclination of diagonal strut on stirrup effectiveness.

5. Models Provided by Other Researchers

As shown in TABLE II, the following models are provided by the Japan Society of Civil Engineering (JSCE) standard (JSCE 1997); CNR DT-203/2006 (Italian Research Council 2007); Hoult et al. 2008; Alam and Hussein 2012; and Kara 2011.

TABLE II

ADDITIONAL SHEAR DESIGN MODELS

Model	Concrete Shear Equations	Transverse Shear Equations
JSCE guidelines (1997)	$V_c = \beta_d \beta_p \beta_n f_{vcd} bd / \gamma_b$ $f_{vcd} = 0.2(f_c^{'})^{\frac{1}{3}} \le 0.72\text{MPa}$ $\beta_d = \left(\frac{1000}{d}\right)^{\frac{1}{4}} \le 1.5$ $\beta_p = \left(100\frac{\rho_{fl}E_{fl}}{E_s}\right)^{\frac{1}{3}} \le 1.5$ $\beta_n = 1 + \frac{M_o}{M_d} \le 2 \text{for} N_f \ge 0$ $\beta_n = 1 + \frac{2M_o}{M_d} \le 2 \text{for} N_f < 0$ $\gamma_d = 1.3$	$V_{\text{fv}} = \frac{\left[\frac{A_{\text{fv}}\sigma_{\text{fv}}(\sin\alpha_s + \cos\alpha_s)}{s}\right] jd}{\gamma_b} \le \frac{f_{\text{FRPbend}}}{E_{\text{fv}}} bd$ $jd = d/1.15$ σ_{fv} is the smaller of $\begin{cases} \frac{\left(\frac{0.05r_b}{d_b} + 0.3\right) f_{\text{fv}}}{1.5} \\ E_{\text{fv}}\varepsilon_{\text{fv}} \end{cases}$ $\varepsilon_{\text{fv}} = 0.0001\sqrt{f_{mcd}^{'} \times \frac{\rho_{\text{fl}}E_{\text{fl}}}{\rho_{\text{fv}}E_{\text{fv}}}}$ $f_{mcd}^{'} = \left(\frac{h}{100}\right)^{-\frac{1}{10}} f_c^{'}$ $\gamma_b = 1.15$

CNR DT-203 (2006)	$V_c \le \begin{cases} V_{\text{Rd,ct}} \\ V_{\text{Rd,ctmax}} \end{cases}$ $V_{\text{Rd,ct}} = 1.3\left(\frac{E_f}{E_s}\right)^{\frac{1}{2}} V_{\text{Rd,c}}$ $V_{\text{Rd,c}} = \tau_{\text{Rd}} k_d (1.2 + 40\rho_{\text{fl}}) bd$ $\tau_{\text{Rd}} = 0.25 f_{\text{ctk0.05}} / \gamma_c$ $f_{\text{ctk0.05}} = 0.05 f_c^{'} \gamma_c = 1.6$ $1.3\left(\frac{E_f}{E_s}\right)^{\frac{1}{2}} \le 1$ If more than 50% of bottom reinforcement is interrupted: $k_d = 1$ If less than 50% of bottom reinforcement is interrupted: $k_d = (1.6 - d), d$ in meters $V_{\text{Rd,ctmax}} = \frac{1}{2} \nu f_{\text{cd}} b 0.9d$ $\nu = 0.7 - f_c^{'} / 200 \ge 0.5$	$V_{\text{fv}} = \frac{A_v f_{\text{fr}} d}{s}$ $f_{\text{fr}} = \frac{f_{\text{fd}}}{\gamma_{f,\varphi}}$ $f_{\text{fd}} = \frac{f_{\text{fv}}}{\gamma_f}$ If no specific experimental tests are performed, and that $\frac{r_d}{d_b} \ge 6$: $\gamma_{f,\varphi} = 2$ If specific experimental tests are performed: $\gamma_{f,\varphi} = \frac{f_{\text{FRPbend}}}{f_{\text{fv}}}$
Hoult et al. (2008)	$V_c = \beta \sqrt{f_c^{'}} b d_v$ $\beta = \frac{0.30}{0.5 + (1000\varepsilon_x + 0.15)^{0.7}} \times \frac{1300}{1000 + s_{ze}}$ $d_v = 0.9d$ $s_{\text{xe}} = \frac{31.5d}{16 + a_g} \ge 0.77d$ $a_g = \begin{cases} a_g, \text{ if } f_c^{'} < 60 \\ a_g - \frac{a_g}{10} \times (f_c^{'} - 60), \text{ if } 60 \le f_c^{'} < 70 \\ 0, \text{ if } f_c^{'} > 70 \end{cases}$ $\varepsilon_x = \frac{\left(\frac{M_f}{d_v}\right) + V_f}{2(E_s A_s)}$	

Alam and Hussien (2012)	$V_{\mathrm{Rd,c}} = \dfrac{0.2\lambda}{\left(a/d\right)^{2/3}}\left(\dfrac{\rho_f E_f}{d}\right)^{\frac{1}{3}}\sqrt{f_c'}\,b_w d$ $\left(\dfrac{0.1\lambda}{a/d}\right)\sqrt{f_c'}\,b_w d \le V_{\mathrm{Rd,c}} \le 0.2\lambda\sqrt{f_c'}\,b_w d$ λ is the concrete density factor f_c' is the concrete compressive strength
Kara (2011)	$V_{\mathrm{Rd,c}} = b_w d\left(\sqrt[3]{\dfrac{d}{a}}\,f_c'\,\dfrac{\rho_f E_f}{E_s}\left(\dfrac{c_1^2}{c_0}\right)\right)^{\frac{1}{3}}\dfrac{c_0}{c_2}$ a is the shear span $c_0 = 7.696$ $c_1 = 7.254$ $c_2 = 7.718$

The study conducted by Machial et al. (2012) compared the various shear provisions developed by ACI , CSA, JSCE, and other researches by conducting the following performance checks; experimental shear strength over calculated shear strength (*x*-values), Coefficient of Variance (COV), and the absolute average error (AAE). Additionally, a performance test was used to compare the efficiency of the considered code equations. Many of the considered code equations were developed using limited experimental data available at the time. The purpose was to verify the performances of the existing standards and model against the current, larger database.

As shown in TABLE III, results from this study concluded are based on a statistical analysis comparing the estimated experimental shear capacity with the shear capacity calculated from select design codes. Higher χ-values indicate conservative estimates for shear capacities and the CSA S806 approach exhibited the best all-around performance in predicting the shear contribution of FRP reinforced beams when compared to other design methods. However, further improvement is possible and needed.

TABLE III

ACCURACY COMPARISON OF DESIGN CODES (Machial et al. 2012)

	χ-value
AASHTO (2009)	1.79
ACI 440 (2006)	1.79
CSA S6 (2006)	3.25
CSA S6 Addendum (2009)	1.49
CSA S806 (2012)	1.19

D. Summary

Overall, the main difference in the presented standards is the account for the angle of inclination of the diagonal concrete struts, θ. The MCFT provides a theoretically sound, simplified method from estimating the angle θ, and was adopted by CSA S806. Because the angle, θ can significantly deviate from 45° with angles as large as 60°, the assumption of 45° in the design equation leads to an overestimate of, V_s, the strength provided by reinforcement (Razaqpur and Spadea 2014). Razaqpur (2014) also reported that by comparing the actual shear strength of beams, with and without FRP shear reinforcement, based on CSA S806 compared to ACI 440, CSA S6-06, JSCE, and Italian CNR guidelines, it was concluded overall that the CSA S806 method gave more accurate results.

However, the basic form of the V_s equation does not account for the potential variation of the stress of the shear reinforcement, f_v depending on the orientation angle, θ. Currently, CSA and other codes try to limit strain regardless of the impact of the orientation angle. Because the GFRP reinforcement is an anisotropic material, the stress, f_v, can vary

significantly depending on the reinforcement orientation. Further research is needed on the maximum shear capacity provided by the reinforcement depending on the crack angle, θ.

III. EXPERIMENTAL PROGRAM

A. Test Matrix

The experimental program of this study was designed to quantify the shear characteristics of GFRP reinforcing bars embedded in concrete. There were many variables to consider that contribute to the shear capacity and mechanisms of GFRP reinforced concrete such as concrete strength (f'_c), shape of reinforcement (i.e. bent or straight bar), type of FRP material, diameter of bar (d_b), and total area of contributing reinforcement (A_{fv}). While variables from previous research included the longitudinal reinforcement ratio (ρ_f), transverse reinforcement ratio (ρ_v), span to depth ratio, and size effect (i.e. depth of beam). Most researchers did not consider the orientation of the internal reinforcement, even though the crack angle, θ, influences the capacity. In addition, previous research relied on the use of traditional beam specimens to determine the behavior of FRP longitudinal and shear reinforcement. While this may provide useful insight into how actual FRP structural elements behave, it may not be the best type of specimen to characterize the fundamental shear behavior of the newer composite reinforcement.

In this study, the main variable investigated was the orientation of the shear reinforcement with respect to the crack plane. The reinforcing bars were placed at varied angles of 45, 90 and 135-degrees embedded in concrete push-off specimens. These orientations of reinforcement mimic the behavior of concrete beams subjected to shearing forces. This test method can provide information on the relationship between crack parameters (i.e., crack width and slip) and shear force contributed by the reinforcement and aggregate interlock. TABLE IV shows the variables used in the test matrix.

TABLE IV

TEST VARIABLES & MATRIX

Materials	Replicate ID	Number of Bars	Angle, θ	Number of Samples
Steel*	I	1	45	1
			90	1
			135	1
GFRP	I, II	1	45	2
			90	2
			135	2
	I, II	2	45	2
			90	2
			135	2
			Total:	15

Note: "*" Steel of Grades 60 and 80

To characterize the shear behavior of GFRP in concrete, fifteen push-off specimens were fabricated and tested in the Civil and Environmental Engineering laboratory at the University of Louisville, Louisville, Kentucky. Of the total number of specimens constructed, six specimens contained a single GFRP bar, while another three specimens contained a single steel rebar of Grades 60 and 80. The steel bars established the control and was the basis for comparative analysis of material behavior. Due to a communication error with the material supplier, steel grades varied. The final six specimens contained two GFRP bars spaced apart approximately three-inches on center.

As shown in FIGURE 6, the nomenclature of the specimen identification (ID) is defined by the first letter (e.g., G or S) representing the type of reinforcement used. The following number (e.g., 1 or 2) identified the number of bars crossing the crack plane and

is succeeded by the replicate ID number (e.g., I or II). Finally, the last designated number is the orientation of the reinforcement with respect to the crack plane.

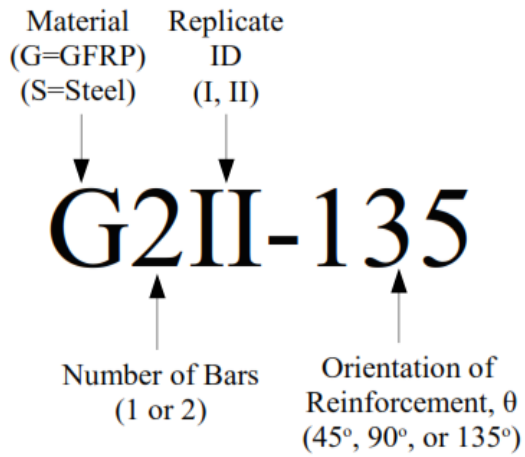

FIGURE 6 – Example of Push-off Specimen Nomenclature

As shown in FIGURE 7, the shear and longitudinal reinforcement in a reinforced concrete beam are representative of the orientation of the reinforcement in the push-off specimens. The shear reinforcement, or stirrups, are modeled by assuming the 135-degree orientation to the shear crack. The bars with the 135-degree orientation are expected to experience tensile forces produced by the applied shear force. Furthermore, the longitudinal reinforcement is typically the 45-degree orientation, and will primarily be under the influence of compressive forces during any slip along the crack. The combination of these two forces are expected to exist in the 90-degree orientation. All three orientations are expected to experience transverse shearing forces with respect to crack slip. However, the amount of transverse shear force resisted varies with bar orientation.

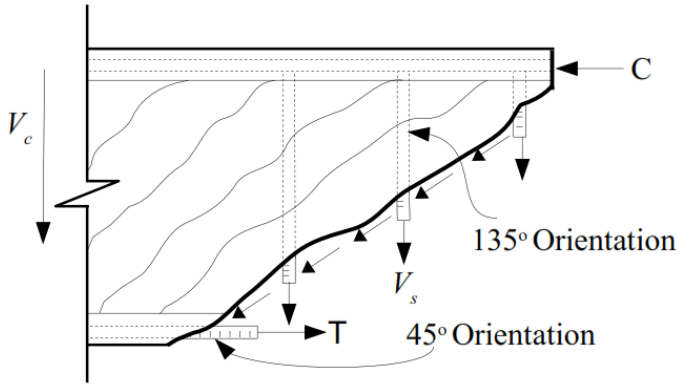

FIGURE 7 – Representative Reinforcement Angles in R.C. Beam

B. Testing Procedures for Material Characterization

1. Mixing and Casting of Concrete

The type of cement used in this study was Type I Portland cement provided by the CEMEX cement plant located in Louisville, Kentucky. As specified by the ACI mix design method (ACI 211.1 1991) for normal weight concrete, the water to cement (w/c) ratio and design strength for the concrete was 0.49 and 4,000 psi, respectively. The concrete was mixed according to ASTM C192, *Standard Practice for Making and Curing Concrete Test Specimens in the Laboratory* (ASTM C192 2012).

The fine and coarse aggregate used was donated by Nugent Sand Company located in Louisville, Kentucky. The fine aggregate (FA) was conventional river sand, and the coarse aggregate (CA) was ⅝ inch river gravel. The river gravel is more rounded as compared to crushed limestone. To determine the physical properties of the aggregates a specific gravity and sieve analysis tests were performed in accordance with ASTM C127, *Standard Test Method for Density, Relative Density (Specific Gravity), and Absorption of Coarse Aggregate*, and ASTM C136, *Standard Test Method for Sieve Analysis of Fine and Coarse Aggregates* respectively (ASTM C127 2013; ASTM C136 2013).

TABLE V

PROPERTIES OF MATERIALS IN CONCRETE

	Cement	FA	CA	Water
Specific Gravity	3.15	2.82	2.5	
Density (lb/ft^3)	196	176	161	
Fineness Modulus	-	2.98	-	Local Tap Water
Dry Rodded Wt. (lb/ft^3)	-	-	99.2	
Absorption Capacity (%)	-	0.8	2.5	

As shown in TABLE V, the absorption capacities of the aggregates were 0.8 and 2.5-percent for fine and coarse aggregate, respectively. The moisture content varied for each concrete batch due to being stored in bulk stockpiles. Moisture content was determined in accordance with ASTM C566, *Standard Test Method for Total Evaporable Moisture Content of Aggregate by Drying* (ASTM C566 2013). The grain size distribution is satisfactory within the upper and lower limits according to ASTM C33, *Standard Specifications for Concrete Aggregates* (ASTM C33 2013), as shown in FIGURE 8.

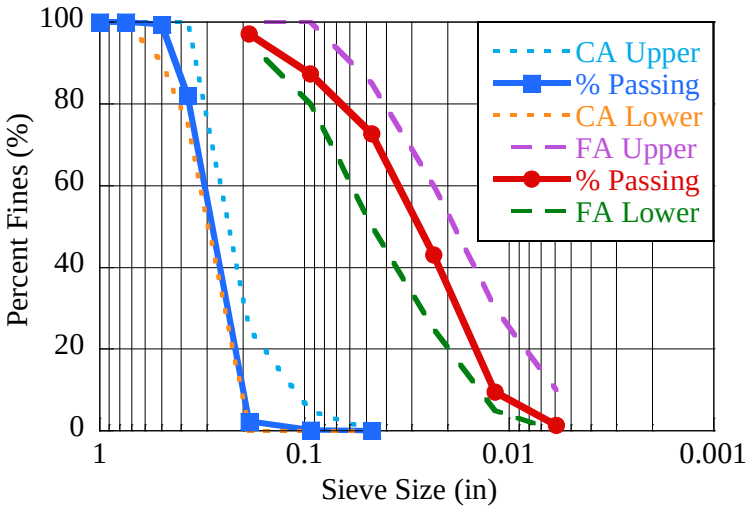

FIGURE 8 – Grain Size Distribution of Aggregates

TABLE VI shows mixture proportions based on one-cubic-yard yield of concrete. Each concrete batch had a volume of approximately three cubic feet to produce a push-off test specimen and six cylinders. The measured slump of fresh concrete was approximately one to two inches for each batch, and was completed according to ASTM C143, *Standard Test Method for Slump of Hydraulic-Cement Concrete* to check the consistency of workability (ASTM C143 2012).

TABLE VI

CONCRETE MIXTURE PROPORTIONS

Material	Weight (lb/yd^3)
Cement	680
Coarse Aggregate	1246*
Fine Aggregate	1741*
Water	335

Note: "*" indicates saturated surface dry (SSD) condition of aggregates.

As shown in FIGURE 9(a), test specimens and cylinders were casted immediately after determining the fresh properties (ASTM C192 2012). After casting, specimens were covered with wet burlap and plastic sheets to cure for the first 24 hours at ambient room temperature, as shown in FIGURE 9(b). Exposed reinforcement was protected with plastic sheeting secured with tape to prevent further moisture infiltration.

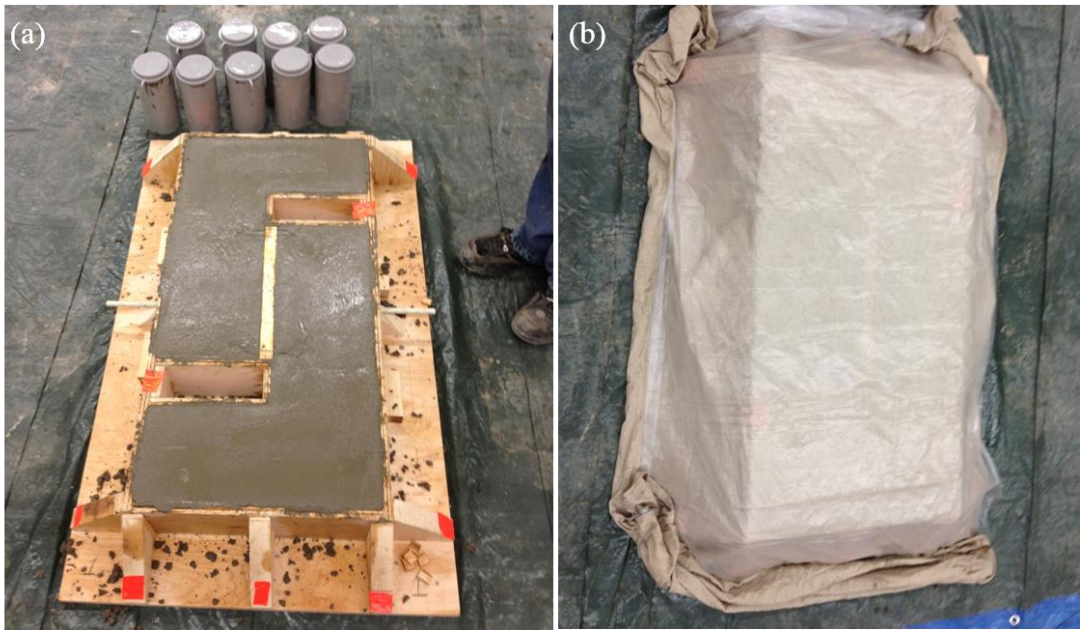

FIGURE 9 – Concrete Casting: (a) Test Specimen and Cylinders; (b) Field Curing

As shown in FIGURE 10, after field curing, samples were covered with burlap and placed in a sealed curing room for 28±1 days, at approximately 75°F with 98% relative humidity. Similarly, concrete cylinders were demolded and placed in limewater bath solution at 72°F for 28±1 days. Prior to testing, the specimens and test cylinders were removed to air dry at ambient room temperature for at least 16 hours.

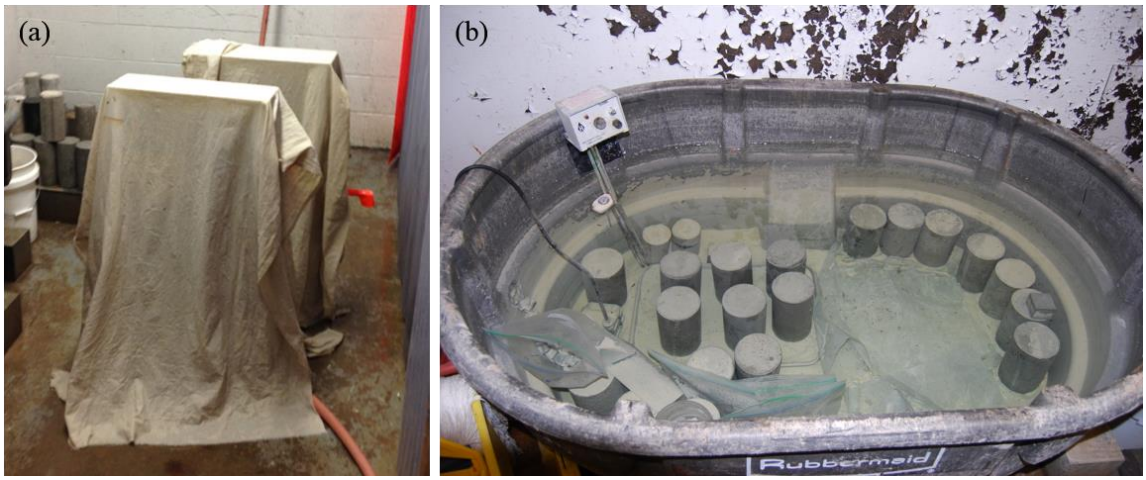

FIGURE 10 – Curing of Specimens: (a) Test Specimen; (b) Cylinder Limewater Bath

2. GFRP Reinforcement

The GFRP bars used throughout this study were provided by Hughes Brothers, Inc. The bars were type E-glass, sand coated, with helically wound ribs, and a nominal diameter of 0.5 inches (Designated as No. 4). Tensile properties were determined in compliance with ASTM D7205, *Standard Test Method for Tensile Properties of Fiber Reinforced Polymer Matrix Composite Bars* (ASTM D7205 2011). Five specimens were tested, each having a length of 55 inches. As shown in FIGURE 11(a), both ends were encased in a galvanized steel pipe and casted with Euro Rock expansive grout, to prevent a crushing failure of the bar. FIGURE 11(b) shows the extensometer, which was placed at the center of the GFRP bar, approximately 10 inches from either anchor.

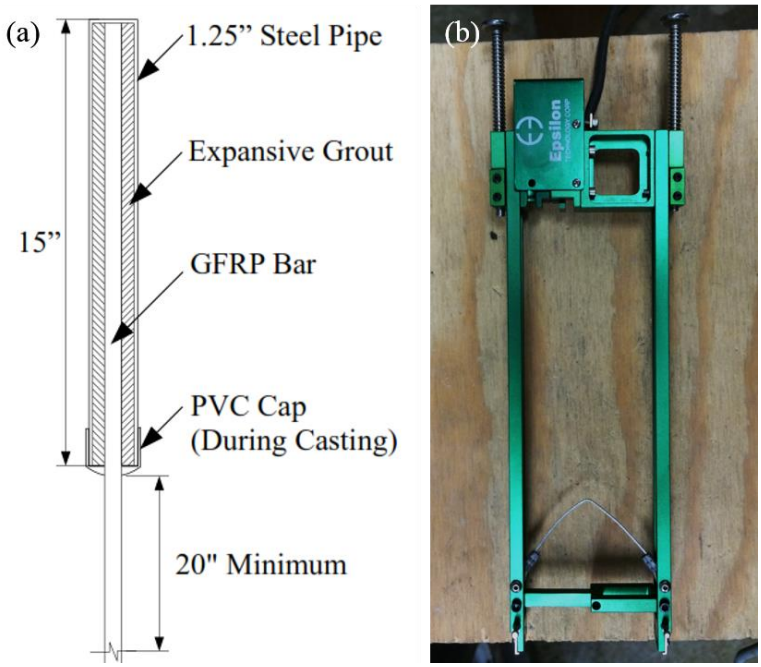

FIGURE 11 – GFRP Tension Specimen: (a) Anchor Details; (b) Extensometer

Once mounted in the 100-kip Universal Testing Machine (UTM), the specimen is monotonically loaded at a constant rate, until failure while recording applied force and longitudinal strain. An adequate rate can be determined by a linear stress-strain plot shown

on the data acquisition system. Prior to failure, the extensometer was removed to avoid damage. Failure of the specimen should occur near the center with no signs of bond degradation resulting in slippage through the anchorage. Values obtained from successful tests are tensile strength and elastic modulus, which is presented in Chapter 4.

3. Mild Steel Reinforcement

The steel reinforcement used was also a #4 bar, with an approximate diameter of 0.5 inches. The mechanical properties of the bar were determined and verified by conducting tension tests conforming to ASTM A370, *Standard Test Methods and Definitions for Mechanical Testing of Steel Products* (ASTM A370 2013). Three specimens obtained from the push-off samples were tested to verify mechanical properties. Each specimen was approximately 8 inches in length, and the nominal diameter was measured to be 0.453 inches. Initial gauge marks were centered 3 in. apart. The steel reinforcing bar was placed in the V-grips of the 60-kip UTM, and loaded until rupture of the bar. After failure, the distance between the two initial gage marks was measured to obtain the percent elongation in order to calculate the modulus of elasticity. Other reported properties include tensile strength, the yield/rupture stresses, and the corresponding strains.

4. Fabrication of Test Specimens

Push-off specimens were fabricated to evaluate the shear characteristics of the GFRP reinforcement embedded in concrete. As shown in FIGURE 12(a), the dimensions of specimens are as follows: 6 inches deep, 18 inches wide and 34.5 inches long. The crack plane was 13.8 inches in length with an area of 82.5 square inches. The orientation of the reinforcement was varied and placed at mid-depth of the specimen with the bar's mid-span at the center of the crack plane. Additional steel reinforcement was provided to protect the

concrete specimen head from premature crushing failure during the push-off test (see FIGURE 12(b)). The reinforcement was a combination of straight and bent No. 4 and 5 rebars. The clear cover was at least one inch measured from every surface.

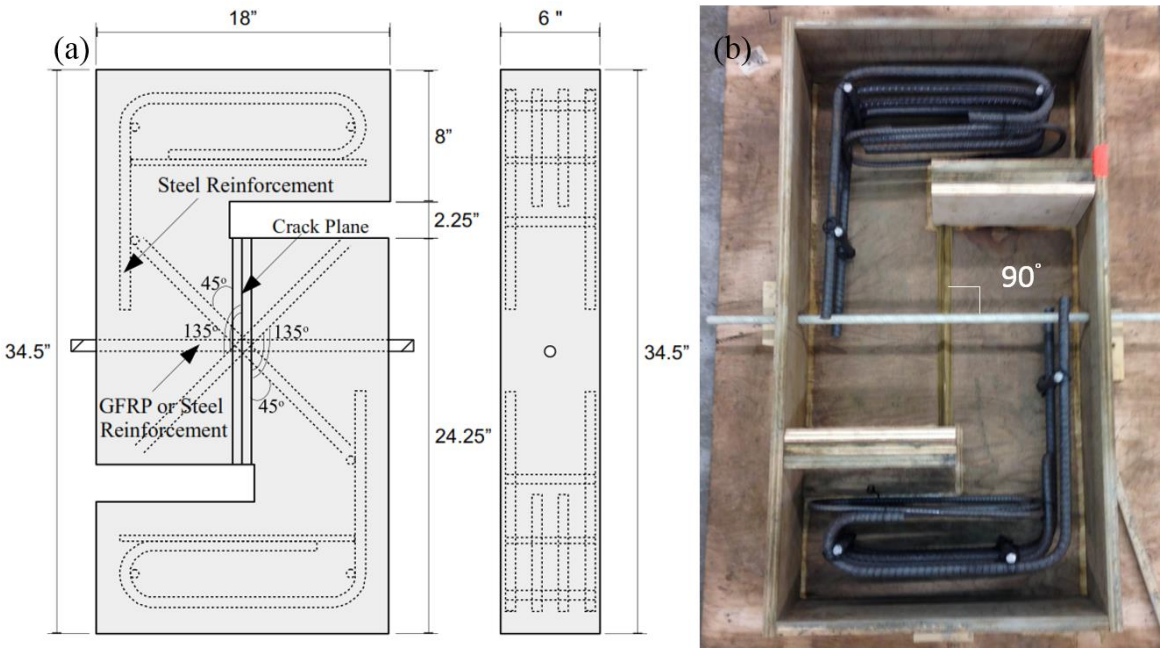

FIGURE 12 – Push-off Specimen: (a) Design (Top and Side View); (b) Formwork and Reinforcement (Top View)

5. Instrumentation

To measure crack width (δ_{CW}) and crack slip (δ_{CS}) displacements, linear variable differential transducers (LVDTs) were mounted on the specimen during the pre-cracking and push-off test. As shown in FIGURE 13(a) the two smaller LVDTs measured $\delta_{CW,}$ and provided a linear range of approximately 0.5 inches. The other two LVDTs measured δ_{CS} with a range of 2 inches. In addition, a standard crack gauge (see FIGURE 13(b)) was used to measure displacements up to approximately ±0.4 inches for crack slip and ±1 inch for crack width.

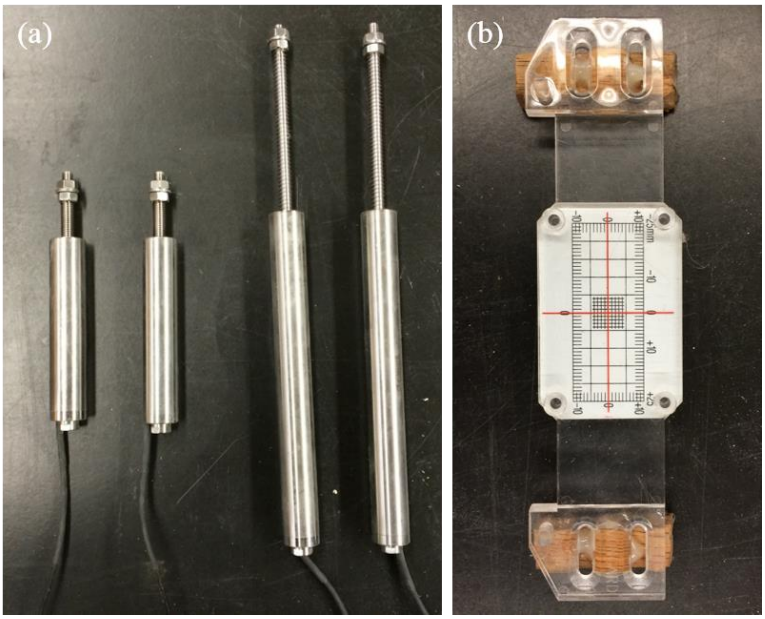

FIGURE 13 – Instrumentation: (a) LVDTs; (b) Standard Crack Gauge

6. Pre-Cracking Test

Testing consisted of two stages, the first being the pre-cracking test. The pre-cracking test creates a crack plane along the length of the specimen that simulates diagonal shear cracks in a concrete beam element. This test is conducted first so the initial crack width condition can be established for the push-off test. The initial δ_{CW} conditions are needed to simulate aggregate interlock between the cracked surfaces and shear force of the reinforcement crossing this plane. As shown in FIGURE 14, pre-cracking was accomplished by applying a line load by two fabricated steel supports on the top and bottom of the specimen at a rate of approximately 0.1 kips per second. To measure initial crack width, a LVDT was placed across the crack plane, at the same location of the reinforcement, along with a standard crack gauge.

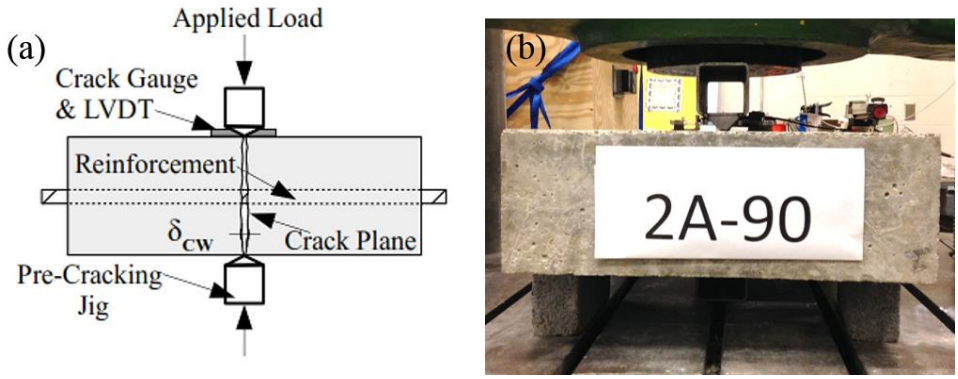

FIGURE 14 – Pre-Cracking Test: (a) Detail; (b) Test Specimen

7. Push-off Test

Following the pre-cracking test was the push-off test. As shown in FIGURE 15, both ends of the specimen contacting the loading apparatus were capped with a quarter-inch of plaster and one inch thick steel plates. This ensured the specimen was on a level surface, in addition to protecting the concrete from premature crushing failure. The loading rate was approximately 0.2 kips per second. Crack width and slip were measured simultaneously during the test with four mounted LVDTs. Two LVDTs were placed along the axis of the reinforcement to measure crack width on either side of the specimen. Crack slip was measured at the top and bottom of the specimen with the other two LVDTs. The 200-kip capacity load cell on the UTM was wired directly to the data acquisition system to acquire the applied force. Testing was terminated when rupture of the GFRP bar occurred, or significant crack width and/or slip exceeded linear ranges of the LVDTs. Results and failure characteristics are discussed in Chapter IV.

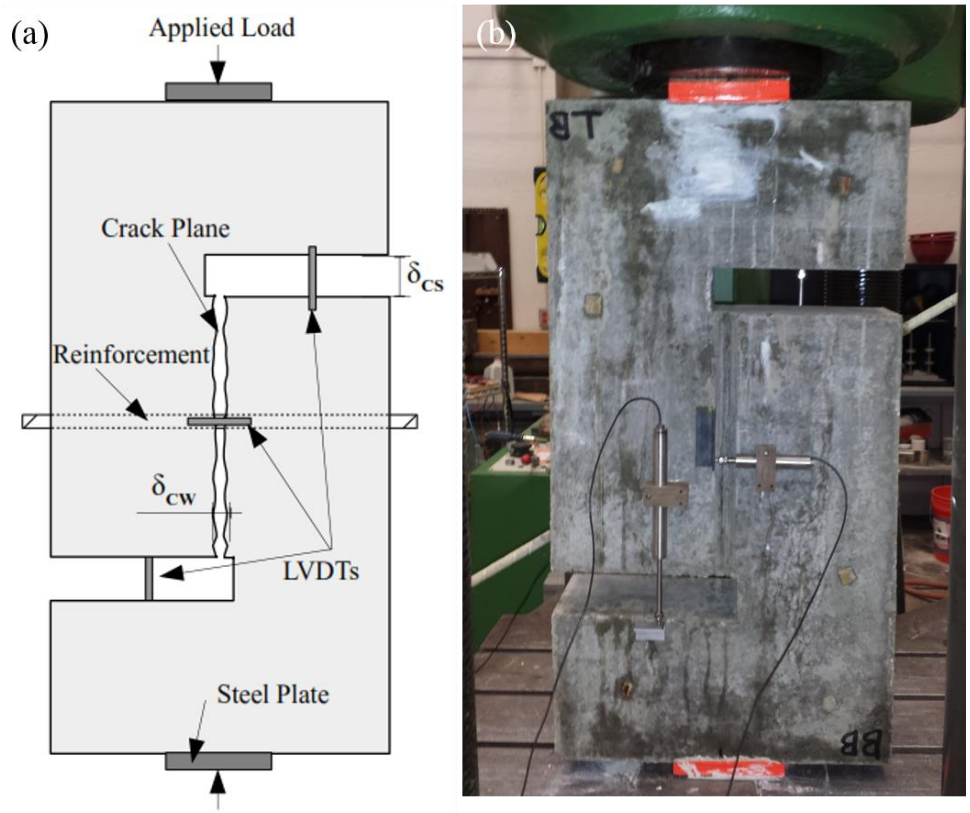

FIGURE 15 – Push-off Test: (a) Detail; (b) Test Specimen (θ = 135°)

8. Compressive and Tensile Strength Tests

Three, four by eight inch (diameter x length) cylinders were tested to determine the compressive and tensile strength of concrete for each batch. Tests were conducted after the completion of push-off tests in accordance with ASTM C39, *Standard Test Method for Compressive Strength of Cylindrical Concrete Specimens*, and ASTM C496, *Standard Test Method for Splitting Tensile Strength of Cylindrical Concrete Specimens*, respectively (ASTM C39 2014; ASTM C496 2011). The results are discussed in Chapter IV.

IV. EXPERIMENTAL RESULTS AND ANALYSIS

A. Mechanical Properties of Materials

1. Concrete

The results from the compressive strength and splitting tensile tests are shown in TABLE VII. The average concrete compressive strength, f'_c, was approximately 6907 psi, with a standard deviation of 345 psi. Using Equation (31), the average tensile strength, f_t, for concrete was calculated as 656 psi, with a standard deviation of 46 psi. FIGURE 15 shows the cylinder failures. The compression specimen exhibited a typical conical failure and splitting failure occurred along the major axis of the tension specimen.

$$f_t = \frac{2P}{\pi l d} \tag{31}$$

TABLE VII

CONCRETE MATERIAL PROPERTIES

	f'_c (psi)	f_t (psi)
Average	6907	656
St. Deviation	345	46
COV	0.05	0.07

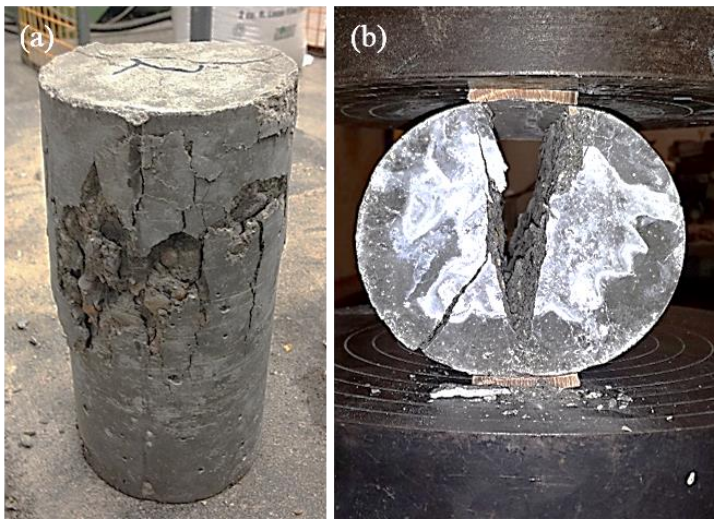

FIGURE 16 – Typical Concrete Cylinder Failure: (a) Compressive Strength Test; (b) Splitting Tensile Test

2. GFRP Reinforcement

The #4, 0.5 inch diameter, GFRP reinforcement was evaluated by conducting tensile tests to determine its mechanical properties in accordance with ASTM D7205 (ASTM D7205 2011). A typical failure of a GFRP tension specimen is shown in FIGURE 17.


FIGURE 17 – Failure of GFRP Tension Specimen

TABLE VIII

TENSILE PROPERTIES OF GFRP REBAR

	Test Results (4 samples) (f_{fu})		Reported by Manufacturer ($f_{fu,ave} - 3\sigma$)	ACI 440 (f_{fu})
Ultimate Tensile Load (kip)	Average	27	21.6	14 - 46
	St. Deviation	0.27		
Tensile Strength (ksi)	Average	136	110	70 - 230
	St. Deviation	1.4		
Elastic Modulus, $x10^3$ (ksi)	Average	7.1	6.7	5.1 - 7.4
	St. Deviation	0.08		

As shown in TABLE VIII, the GFRP bars had an ultimate tensile load of 27 kip (St. Deviation of 0.27), tensile strength of 137 ksi (St. Deviation of 1.4), and an elastic modulus of $7.1x10^3$ ksi (St. Deviation of 0.08). The values exceed the guaranteed ultimate tensile strength (GUTS) reported by the manufacturer and are within the range specified by ACI 440 (2006). GUTS is calculated as the mean tensile strength, $f_{fu,ave}$, minus three times the standard deviation ($f^*_{fu} = f_{fu,ave} - 3\sigma$). The guaranteed strength values provide a 99.87% probability that similar FRP bars exceed the indicated values, if at least 25 specimens are tested (Dally and Riley 1991). FIGURE 18 shows a typical stress-strain plot of a GFRP tension specimen.

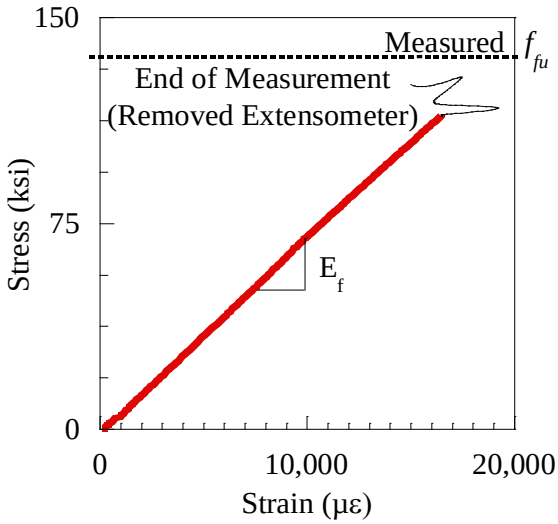

FIGURE 18 – Typical GFRP Stress-Strain Curve

3. Mild Steel Reinforcement

The mild steel reinforcement was a #4 (0.5 inch diameter) bar and evaluated by conducting tension tests in accordance with ASTM A370 (ASTM A370 2013). FIGURE 19 shows a typical rupture for a steel tension specimen indicating a successful test.


FIGURE 19 – Failure of Steel Tension Specimen

TABLE IX

TENSILE PROPERTIES OF STEEL REBAR

	Reported Average Values		ASTM A615 (Minimum Requirements)	
	Grade 60*	Grade 80^{+}	Grade 60	Grade 80
Yield Stress, f_y (ksi)	66	90	60	80
Yield Strain, ε_y (in/in)	0.0027	0.0052	-	-
Rupture Stress, f_u (ksi)	108	105	90	105
Rupture Strain, ε_u (in/in)	0.166	0.115	-	-
Elastic Modulus, E_s x10^3 (ksi)	29	30	-	-

Note: "*" 2 samples; "$^{+}$" 1 sample; "-" indicates no requirement

As shown in TABLE IX, the Grade 60 steel bars had an average yield stress of 66 ksi, yield strain of 0.0027 in./in., an average rupture stress of 108 ksi, an average rupture strain of .166 in./in., and an average elastic modulus of 29x10^3 ksi. The Grade 80 steel rebar had a yield stress of 90 ksi, yield strain of 0.0052 in./in., rupture stress of 105 ksi, rupture strain of .115 in./in., and an elastic modulus of 30x10^3 ksi. Both grades exceeded the minimum requirements of ASTM A615 (ASTM A615 2014) indicating satisfactory material properties. FIGURE 20 shows the typical stress-strain plots for steel tension specimens.

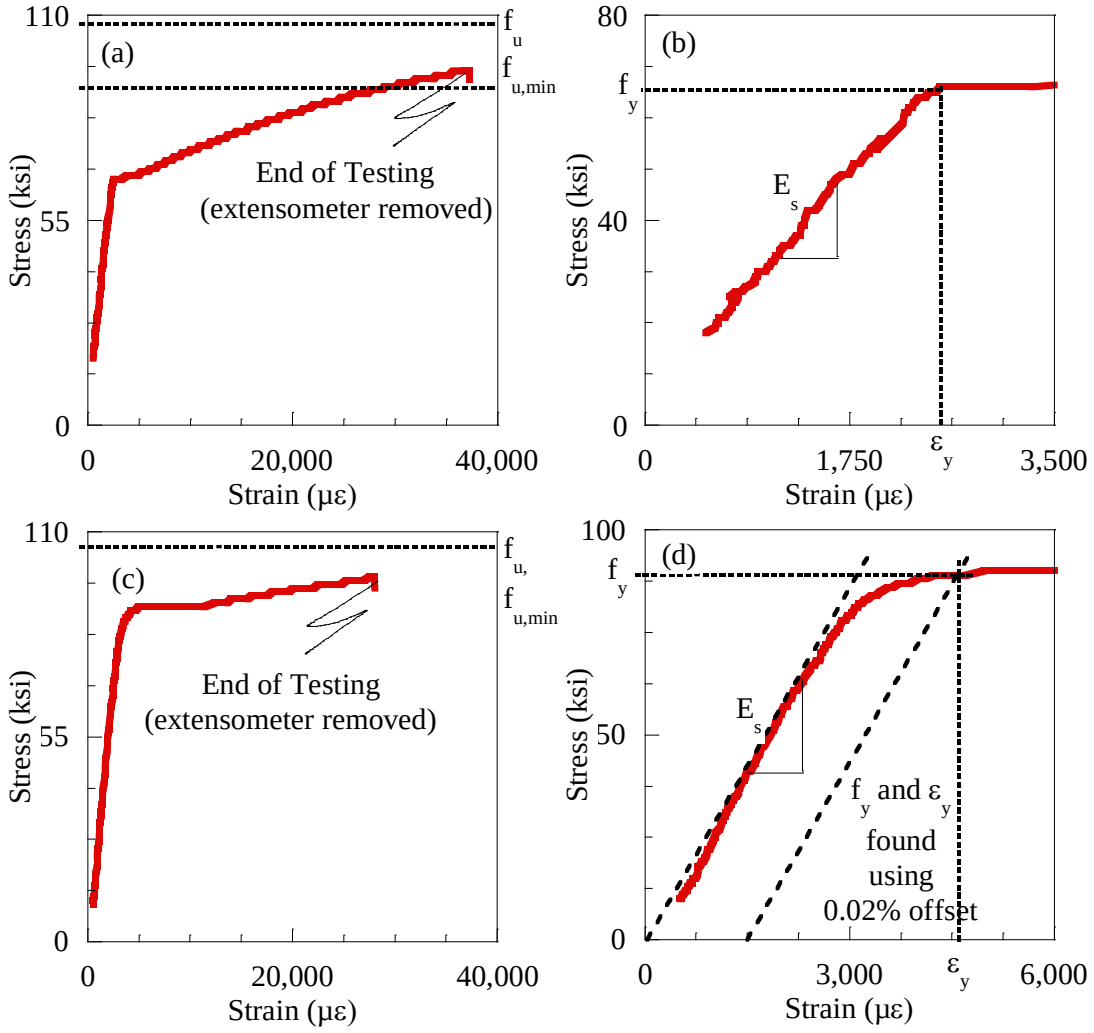

FIGURE 20 – Steel Stress-Strain Curves: (a) f_u and $f_{u,min}$ (Grade 60); (b) E_s, f_y, and ε_y (Grade 60); (c) f_u and $f_{u,min}$ (Grade 80); (d) E_s, f_y, and ε_y (Grade 80)

B. Failure Mechanisms

There were three modes of failure observed during the push-off tests. The first failure mode was caused by compressive forces, the second by tensile, and the third mode was a combination of the first two modes. Tensile failure was observed for samples with the 135-degree bar orientation (i.e., S1E-135 and G1I-135), compressive failure in the 45-degree specimens (i.e., G1I-45), and a combination of tension and compression in the 90-degeree

specimens (i.e., G1I-90). The following subsections describe in detail the behavior of GFRP and steel reinforcement.

1. Observations of GFRP Reinforcement Rupture

As shown in FIGURE 21, each mode suggests different stresses formed in the GFRP matrix and fibers, causing different failure modes. The 45-degree orientation leads to compressive and shear stresses in the GFRP, resulting in buckling and a kinking effect (shown by the separation of fiber layers), and leads to significantly lower shear capacities (See FIGURE 21(a)). The 135-degree specimen's bar failure is categorized as Mode II (See FIGURE 21(b)). Failure is characterized with high-tension forces in the fibers until the maximum applied force is reached during the push-off test. Similar to the bar tension tests, tensile forces stretched the bar fibers along its primary axis, causing abrupt failure and producing the highest shear capacities for this reinforcement. The mixed failure mode (tension and compression) was exhibited in the 90-degree orientation. Fibers along the top surface of the bar were jagged (similar to Mode II), while along the bottom surface, the fibers remained bunched together but separated in distinctive layers (similar to Mode I) (See FIGURE 21(c)).

FIGURE 21 – Failure Modes: (a) Mode I, 45°; (b) Mode II, 135°; (c) Mixed Mode, 90°

2. Observations of Steel Reinforcement Rupture

Unlike the GFRP reinforced specimens and the varying grades of steel, the steel reinforced specimens did not exhibit different failure modes based on the bar orientation. However, a complete bar rupture was observed in the 135-degree specimen. The 45 and 90-degree bar only deformed due to significant crack slip displacement. FIGURE 22 shows the extracted steel reinforcement following the push-off test. There was no sign of bond failure.

FIGURE 22 – Steel Failure and Deformation: (a) 135°; (b) 45°; (c) 90°

C. Pre-Cracking Results

1. One Reinforcing Bar System

The influence of crack angle on the pre-cracking force and initial crack width are compared regardless of reinforcement type. The pre-cracking force is dependent on the tensile strength of concrete. Therefore, the reinforcement type and angles are not considered as a major factor to influence the pre-cracking force. As shown in TABLE X, the applied pre-cracking force ranged from 27 to 38 kips. Initial crack widths varied for each specimen from 0.019 to 0.067 inches. For all specimens, the average pre-cracking force and initial crack width was 32 kips and 0.034 inches, respectively. The average

concrete tensile strength for the single bar specimens was 629 psi, with a standard deviation of 40 psi. The low value of COV indicates that tests results are consistent and that the bar orientation has a minimal impact on the pre-cracking force, but this is not the case for the initial crack width.

TABLE X

PRE-CRACKING RESULTS FOR SPECIMENS CONTAINING ONE-BAR

Angle, θ	Specimen ID	Pre-Cracking Force (kip)	Initial Crack Width (in.)	f_t (psi)
45	G1I-45	30	0.067	621*
	G1II-45	27	0.056	607
	S1I-45	31	0.019	592
90	G1I-90	33	0.021	696
	G1II-90	28	0.026	643
	S1I-90	35	0.025	576
135	G1I-135	33	0.023	613
	G1II-135	36	0.046	665
	S1I-135	33	0.022	639
Average		32	0.034	629
St. Deviation		3	0.018	40
COV		0.095	0.524	0.063

Note: "*" Calculated

2. <u>Two Reinforcing Bars System</u>

TABLE XI shows pre-cracking results for reinforced specimens containing two bars. The addition of another bar had no significant effect on the pre-cracking force. Similar to specimens with a single reinforcing bar, the pre-cracking force seems to be dependent on concrete's tensile strength. The average pre-cracking force was approximately 30 kips, with a standard deviation of 3.8 kips and COV of 0.13. The pre-cracking force differs due to the varying tensile strength of concrete. The average initial crack width was found to be 0.034 inches, which is the same as specimens reinforced with one bar. The average tensile

strength of concrete was slightly higher with a value of 691 psi and standard deviation of 28 psi.

TABLE XI

PRE-CRACKING RESULTS FOR SPECIMENS CONTAINING TWO-BARS

Angle, θ	Specimen ID	Pre-Cracking Force (kip)	Initial Crack Width (in.)	f_t (psi)
45	G2I-45	35	0.057	706
	G2II-45	25	0.021	718
90	G2I-90	30	0.012	706
	G2II-90	26	0.024	712
135	G2I-135	29	0.058	645
	G2II-135	35	0.032	659
Average		30	0.034	691
St. Deviation		3.8	0.018	28
COV		0.13	0.518	0.04

D. Push-off Results

1. One Reinforcing Bar System

In general, the orientation angle and type of reinforcement had a significant impact on the applied shear force and displacement with respect to crack width and crack slip. TABLE XII presents the results from the push-off test on specimens containing one reinforcing bar. Also shown is the calculated shear stress with respect to the area of the crack plane. This represents the transferred applied shear stress across the crack through aggregate interlock and includes doweling effects. As the orientation angle increases from 45 to 135-degrees, the applied shear force also increases. In the 45-degree orientation, the peak shear force of GFRP reinforced specimens was 4 kips, which is approximately 60% lower than the steel reinforced specimen. The steel specimen, S1I-90, in the 90-degree

orientation exhibited a peak shear capacity of 29 kips. This is approximately 30% higher when compared to the 90-degree GFRP reinforced specimens; which exhibited peak shear capacities of 22 and 23 kips. The highest peak shear capacities were observed in the 135-degree orientation of the one-bar specimens. The shear capacity of the steel reinforced specimen 18% higher than specimens reinforced with GFRP. For each case of bar orientation, specimens with steel reinforcement exhibited the higher shear capacities compared to GFRP.

TABLE XII

PUSH-OFF RESULTS FOR SPECIMENS CONTAINING ONE-BAR

Angle, θ	Bar Type	Specimen ID	Peak Shear Force (kip)	Peak Shear Stress (ksi)	Crack Width (in.)	Crack Slip (in.)
45	GFRP	G1I-45	4	0.045	0.290	0.578
		G1II-45	4	0.053	0.239	0.249
	Steel	S1I-45	11	0.134	0.275	0.378
90	GFRP	G1I-90	22	0.263	0.096	0.303
		G1II-90	23	0.278	0.090	0.336
	Steel	S1I-90	29	0.347	0.237	0.600
135	GFRP	G1I-135	29	0.348	0.071	0.202
		G1II-135	34	0.408	0.079	0.223
	Steel	S1I-135	38	0.457	0.121	0.418

FIGURE 23(a) through (c) show the applied shear force versus crack width, and FIGURE 23(d) through (f) show the applied shear force versus crack slip. The asterisk indicates rupture of the bar. As shown in FIGURE 23 (b) and (c), the trend up to the peak shear force differs between steel and GFRP reinforced specimens. Steel reinforced specimens exhibited little to no increase in both crack width and slip as applied shear force increase up to the peak. This is attributed to the stiffness of the steel reinforcement, and is

represented by the high modulus of elasticity of steel (E_s = 29x10^3 ksi). Conversely, in the GFRP reinforced specimens, crack width and slip began to increase at approximately 60% of the peak shear force. The low modulus of elasticity of GFRP (E_f = 7.1x10^3 ksi) is attributed to this behavior. The slopes of the two different trends, mimics the mechanical properties of the reinforcement. For example, steel specimens exhibited steeper response slopes compared to GFRP reinforced specimens. The GFRP reinforced specimens at the 90 and 135-degree orientation exhibited peak shear forces similar to the strength values obtained from tension testing. This indicates full performance of the reinforcement without bond failure.

The post-peak behavior also resembles the behavior of a bare bar subjected to tensile force. For example, in the steel reinforced specimens, there was significant displacement after the observed peak shear force, indicating ductile or plastic-elastic behavior. Failure occurs well after the peak as crack width and slip increases, offering a warning sign that failure is about to occur. On the other hand, as crack width and slip increase, GFRP reinforced specimens do not offer significant warning before failure. Because GFRP does not exhibit yielding, abrupt and brittle failures occur shortly after the peak shear force.

While the previously described behaviors were observed in the 90 and 135-degree orientation, a different trend was observed in the 45-degree specimens. This orientation drastically affected the shear capacities. As crack width and slip increase, the GFRP reinforcement contributed to shear capacity with mainly compressive forces acting on the bar. Confining efforts are also affected by the bar orientation and can be observed from the relationship between crack width and slip.

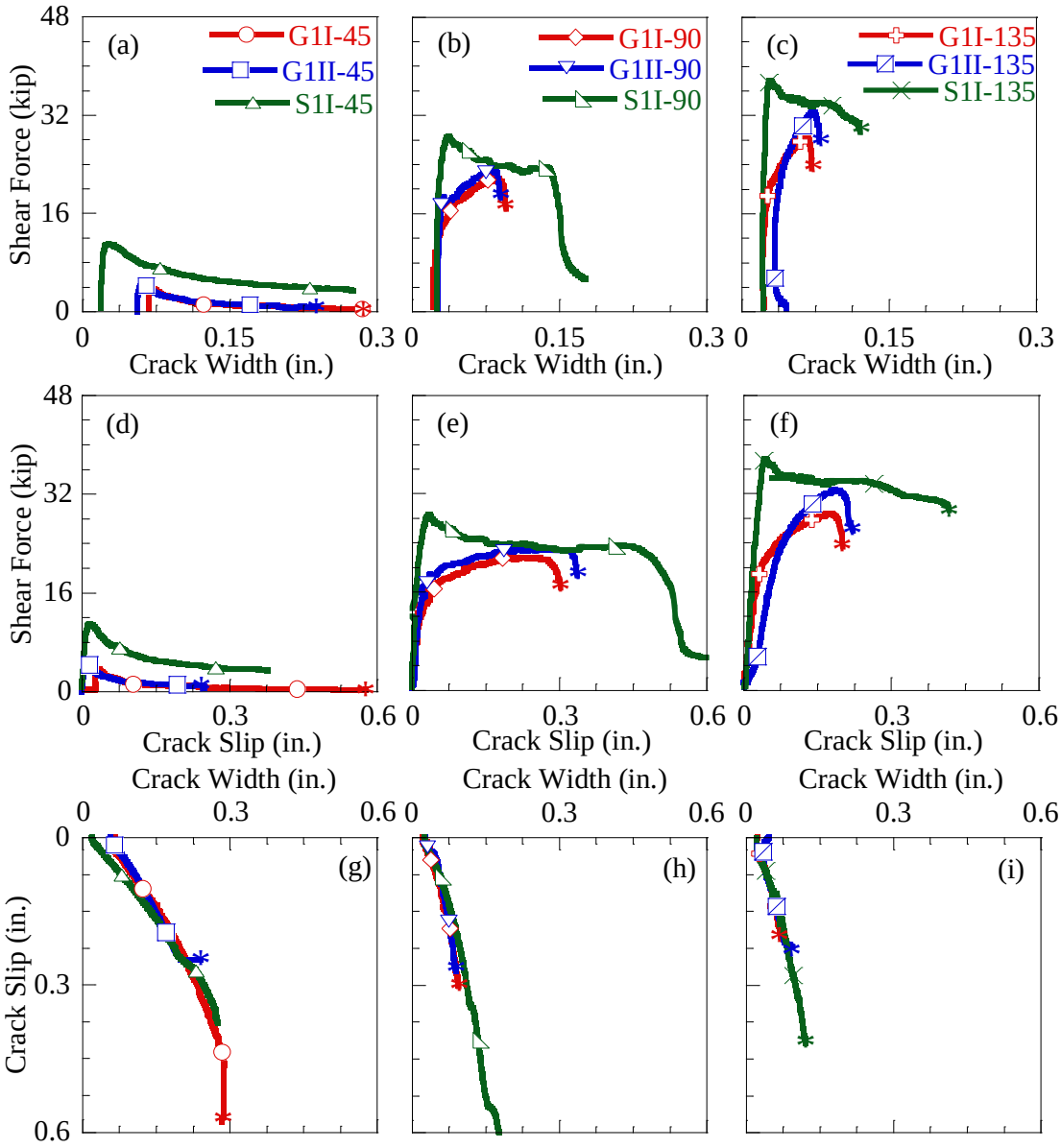

FIGURE 23 – One-Bar Push-Off Plots: (a-c) Shear Force vs. Crack Width; (d-f) Shear Force vs. Crack Slip; (g-i) Crack Slip vs. Crack Width

FIGURE 23(g) through (i) show the crack parameters, crack slip versus crack width. The trends are dependent on the bar orientation rather than bar type. The orientation angle also determined the amount of shear capacity provided by concrete through aggregate interlock. Aggregate interlock is more prevalent in specimens with smaller crack width.

Conversely, specimens with larger crack openings allows more stress to be applied on the reinforcement crossing the crack plane.

For a given value of crack slip or crack width, the 45-degree specimens exhibited larger crack displacements when compared to the other orientations. The 45-degree orientation had an approximate slope of 1:1 (crack width to crack slip ratio), while the 90 and 135-degree orientations had slopes nearing 1:2. Lower slopes (e.g., 1:1) indicate simultaneous crack width and slip, while higher slopes (e.g., 1:2) show larger displacements in crack slip compared to crack width. Larger slopes also show that more confinement is provide by the reinforcement, allowing for smaller crack widths and more resistance provided by aggregate interlock and/or reinforcement. The 90 and 135-degree orientation seems to allow for full performance of the reinforcement. It is clear that the bar orientation is also an important design parameter with respect to the crack plane. Depending on the bar orientation, aggregate interlock as a function of crack width and slip varied significantly, resulting in changes to the shear capacity. The reinforcement experiences more stresses and strains when the orientation is aligned to promote more aggregate interlock. However, the bar properties did not change the path of aggregate interlock (i.e., the relationship between crack width and crack slip).

2. Two Reinforcing Bars

With the addition of a reinforcing bar, an increase in shear capacity was expected depending on the group effect. The group effect occurs when the capacity of two or more reinforcements change the overall capacity of the system positively or negatively. For example, if a specimen is reinforced with one bar which has a capacity of 20 kips, the addition of another bar should increase the system's capacity to 40 kips, if the system is

not affected by the group effect. The additional capacity provided is not expected to affect the crack parameters. TABLE XIII shows the results from the push-off tests on specimens with two GFRP reinforcing bars.

TABLE XIII

PUSH OFF RESULTS FOR SPECIMENS CONTAINING TWO-BARS

Angle, θ	Specimen ID	Peak Shear Force (kip)	Peak Shear Stress (ksi)	Crack Width (in.)	Crack Slip (in.)
45	G2I-45	6	0.077	0.335	0.586
	G2II-45	6	0.075	0.235	0.441
90	G2I-90	35	0.424	0.222	1.082
	G2II-90	34	0.406	0.265	1.323
135	G2I-135	42	0.505	0.264	0.624
	G2II-135	45	0.542	0.274	0.998

When compared to the push off results from specimens with one bar, the shear capacities are higher. The 45-degree specimens obtained a peak shear force of 6 kips, which is 30% higher than the single bar specimens. As mentioned previously, the 90 and 135-degree orientations provide conditions that are more favorable, allowing for full strength utilization of GFRP reinforcement. The 90-degree specimens exhibited a peak shear force of approximately 35 kip, which is a 52% increase in shear capacity from using a single bar. As in specimens with one bar, the 135-degree orientation exhibited the greatest capacity with a value of 44 kips.

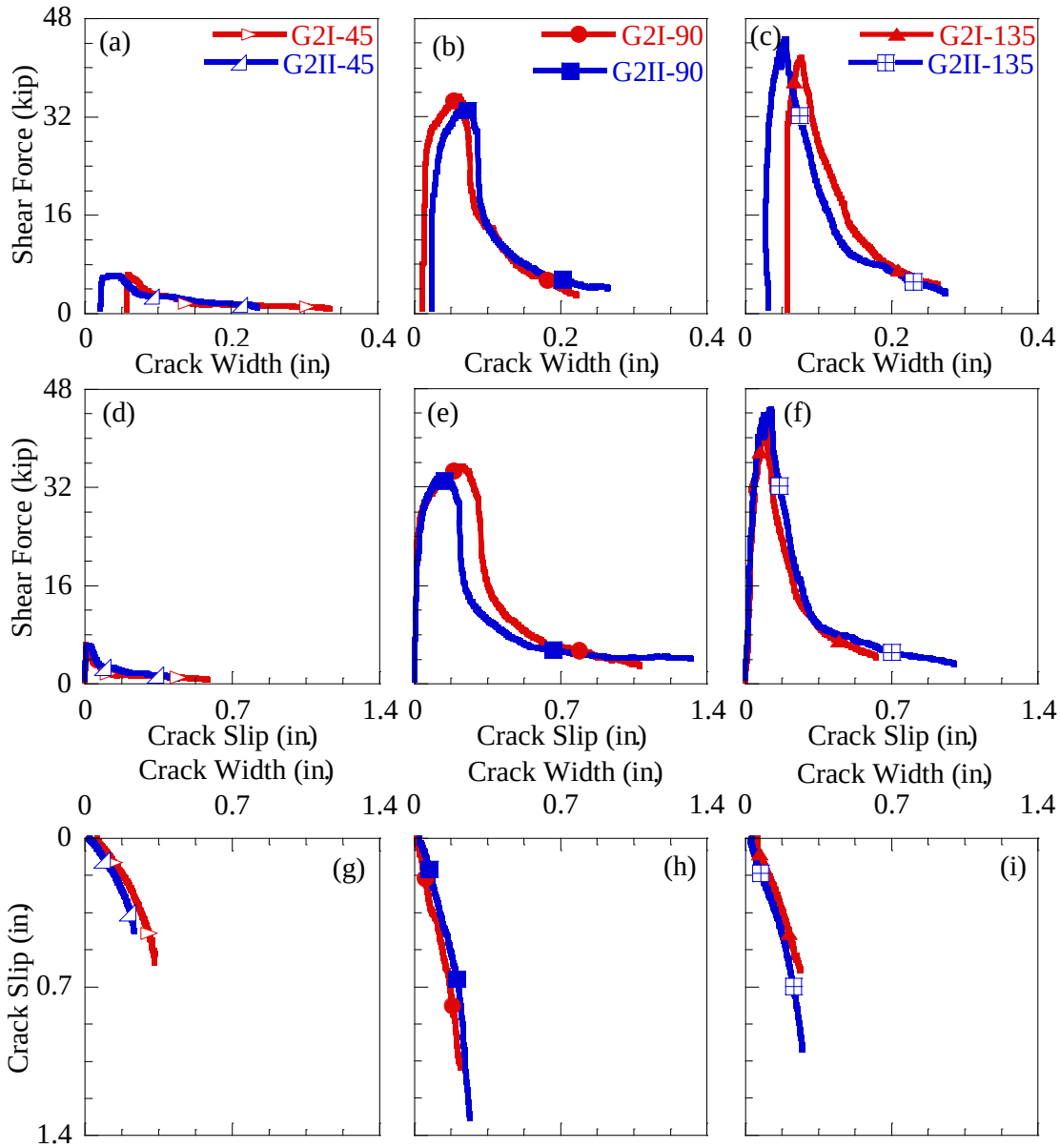

FIGURE 24 - Two-Bar Push-Off Plots: (a-c) Shear Force vs. Crack Width; (d-f) Shear Force vs. Crack Slip; (g-i) Crack Slip vs. Crack Width

FIGURE 24(a) to (c) and (d) to (f) show the applied shear force versus crack width and shear force versus crack slip, respectively. As described during the one bar analysis, the trend for GFRP reinforced specimens mimic the elastic behavior of GFRP reinforcement subjected to tension. The trend up to the peak shear force is similar to the

one-bar specimens. The 45-degree orientation does not provide adequate confinement and due to the brittleness of the GFRP reinforcement, this orientation does not allow for full performance of the bar. The 90-degree specimens exhibited no increase in crack width or slip until 80% of the peak was reached. The 135-degree specimens had a different response up to the peak shear force. As the shear force increased, crack width slightly decreased or remained constant (see FIGURE 24(c)). This can be attributed to the lower stiffness of GFRP reinforcement. Post-peak behavior also differed from specimens with a single reinforcing bar. The 135-degree specimens have a sharp drop off immediately after the peak shear force (see FIGURE 24(c) and (f)). The slope indicates rupture of the reinforcement. However, only one reinforcing bar completely failed while the other bar suffered partial failure. After the completion of testing, the intact fibers were cut to remove the sample from the testing machine. FIGURE 25 shows the failure of the 135-degree two-bar specimen.

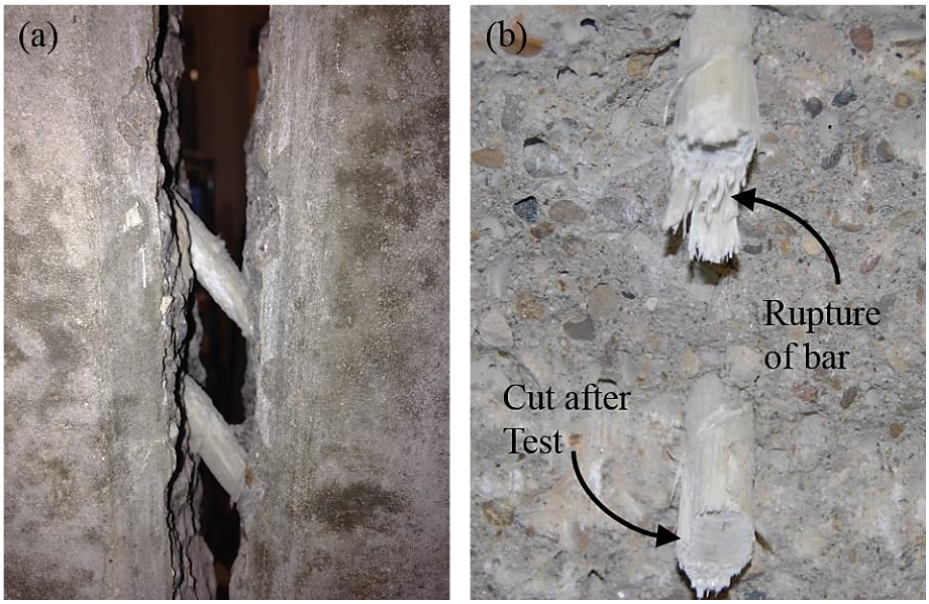

FIGURE 25 – Failure of 135-degree Two-Bar Specimen: (a) Prior to Peak Shear Force; (b) After Peak Shear Force

Longitudinal splitting cracks began forming around the reinforcement in the 90-degree specimens just before reaching the peak shear force. After the peak shear force, the rate of the crack width increased as the splitting cracks propagated, and the bond between concrete and the bar degraded until total bond failure occurred. Failure of the two-bar, 90-degree specimen is shown in FIGURE 26 below.

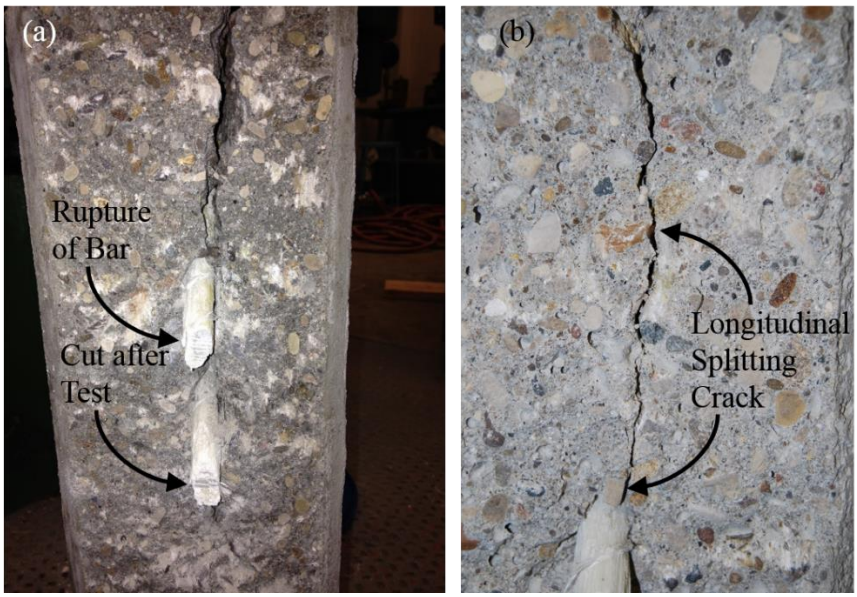

FIGURE 26 – Failure of 90-degree Two-Bar Specimen: (a) Rupture of Reinforcement; (b) Longitudinal Splitting Crack

The 45-degree specimen with two reinforcing bars exhibited the lowest shear capacity. It is definitive that this orientation does not provide adequate confinement to promote friction between the two sliding faces, and this causes a drastic reduction in capacity. At the peak shear force, a plateau was observed, followed by a steady increase in crack width and slip as the applied force decreased. This indicates rupture of the reinforcement. The 45-degree orientation also exhibited failure of both reinforcing bars. This is due to the high compressive forces associated with this orientation. FIGURE 27 shows the complete failure of the specimens containing two-bars oriented at 45-degrees.

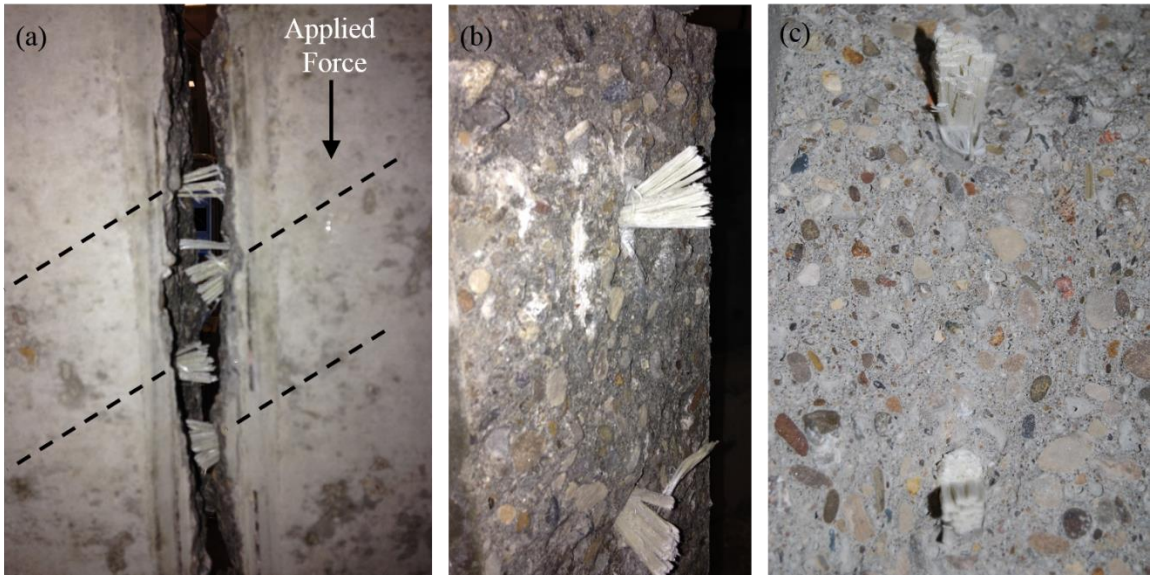

FIGURE 27 – Failure of 45-degree Two-Bar Specimen: (a) Side View of Crack Plane Specimen G2I-45; (b) Crack Plane of Specimen G2I-45; (c) Crack Plane of Specimen G2II-45

FIGURE 24(g) through (i) show the crack parameters crack slip versus crack width. As mention previously, trends are dependent on the bar orientation. The orientation angle also determines the amount of shear capacity provided by concrete through aggregate interlock. For a given value of crack slip or crack width, the 45-degree specimens exhibited larger crack displacements when compared to the other orientations. Slopes were 1:1, 1:3, and 1:2 for the 45, 90, and 135-degree orientations, respectively. Lower slopes (e.g.,1:1) are the indication of simultaneous crack width and slip, while steeper slopes (e.g., 1:2, 1:3) show larger values of crack slip compared to crack width. Larger slopes also indicate that more confinement is provided by the reinforcement, allowing for smaller crack widths and more resistance provided by aggregate interlock.

E. Absorbed Energy

1. Definition of Concept

As shown in FIGURE 28, the concept of absorbed energy is defined as the area under the applied shear force versus crack slip curve. The amount of energy (area) under the curve is representative of the contributions provided by aggregate interlock and the reinforcement.

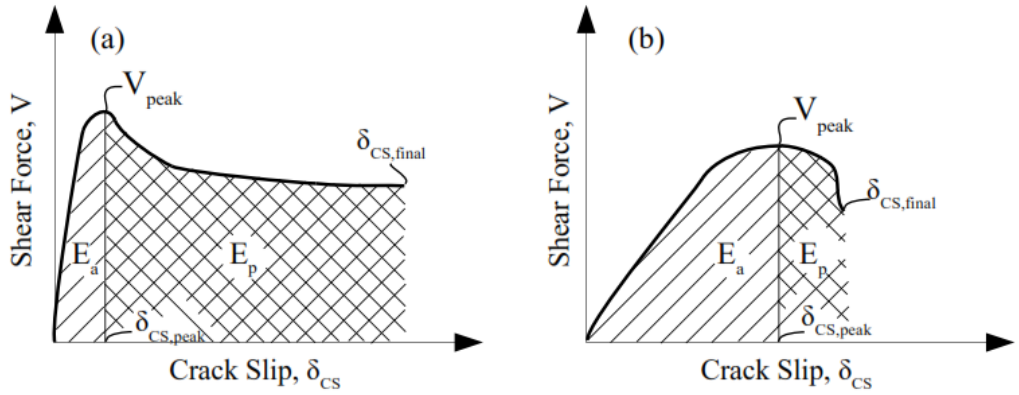

FIGURE 28 – Concept of Absorbed Energy: (a) Typical Steel Specimen; (b) Typical GFRP Specimen

The type of reinforcement shows significant differences for absorbed energy up to the peak shear force and onto the final crack slip value. The applied shear force, V, multiplied by the corresponding crack slip, is integrated to determine the absorbed energy for pre and post-peak. This provides a quantifiable comparable assessment of the amount energy absorbed by aggregate interlock and reinforcement at a specified value of crack slip (Kim et al. 2010). The total absorbed energy, E_T, is calculated as follows:

$$E_T = E_a + E_p = \int_0^{\delta_{CS,final}} V(\delta)\mathrm{d}\delta \tag{32}$$

where E_a and E_p are defined as the absorbed energy up to the peak shear force and the absorbed energy post-peak, from $\delta_{CS,peak}$ to $\delta_{CS,final}$, respectively, and $\delta_{CS,final}$ is the

maximum crack slip corresponding to failure of the bar. The sum of these two parameters yields the total absorbed energy, $E_{T,}$ by concrete through aggregate interlock and the reinforcement.

2. Analysis

TABLE XIV shows the calculated absorbed energy for the peak applied shear force (V_{peak}), the peak crack slip ($\delta_{CS,peak}$), and the final crack slip value ($\delta_{CS,peak}$).

TABLE XIV

ABSORBED ENERGY DUE TO AGGREGATE INTERLOCK

Bar Type	Number of Bars	Specimen ID	V_{peak}	$\delta_{cs,peak}$	$\delta_{cs,final}$	E_a	E_p	E_T
Steel	1	S1I-45	11	0.016	0.378	0.13	1.89	2.02
		S1I-90	29	0.035	0.600	0.74	12.15	12.89
		S1I-135	38	0.044	0.418	0.92	12.47	13.39
GFRP	1	G1I-45	4	0.031	0.578	0.03	0.45	0.479
		G1II-45	4	0.009	0.249	0.03	0.40	0.429
		G1I-90	22	0.258	0.303	4.84	0.92	5.76
		G1II-90	23	0.262	0.336	5.31	1.67	6.98
		G1I-135	29	0.176	0.202	4.00	0.73	4.73
		G1II-135	34	0.185	0.223	3.99	1.16	5.15
	2	G2I-45	6	0.008	0.586	0.03	0.93	0.962
		G2II-45	6	0.023	0.441	0.13	0.91	1.04
		G2I-90	35	0.224	1.081	6.84	8.65	15.49
		G2II-90	34	0.119	1.323	3.25	10.20	13.45
		G2I-135	42	0.100	0.624	2.78	6.66	9.44
		G2II-135	45	0.123	0.998	4.02	8.71	12.73

The reinforcement orientation, type, and number of bars significantly affected the absorbed energy and contribution of concrete by aggregate interlock. Larger absorbed energy indicates ductile behavior, and smaller E-values corresponds to brittle behavior of

the reinforcement. In general, except for specimen G2I-90, steel reinforced specimens exhibited the largest absorbed energy for specimens with a single reinforcing bar within each orientation group. In specimens reinforced with one GFRP bar, more displacement occurring before the peak shear force leads to higher E_a values (e.g., G1-90 series). As shown in TABLE XIV, even though the 135-degree specimens (e.g., G1-135 series) had higher shear capacities, the 90-degree specimens (e.g., G1-90 series) had more energy contribution provided by aggregate interlock and reinforcement. This is attributed to the orientations susceptibility to crack slip and higher confinement of the reinforcement. In specimens reinforced with two GFRP bars, the same trend is obviously observed.

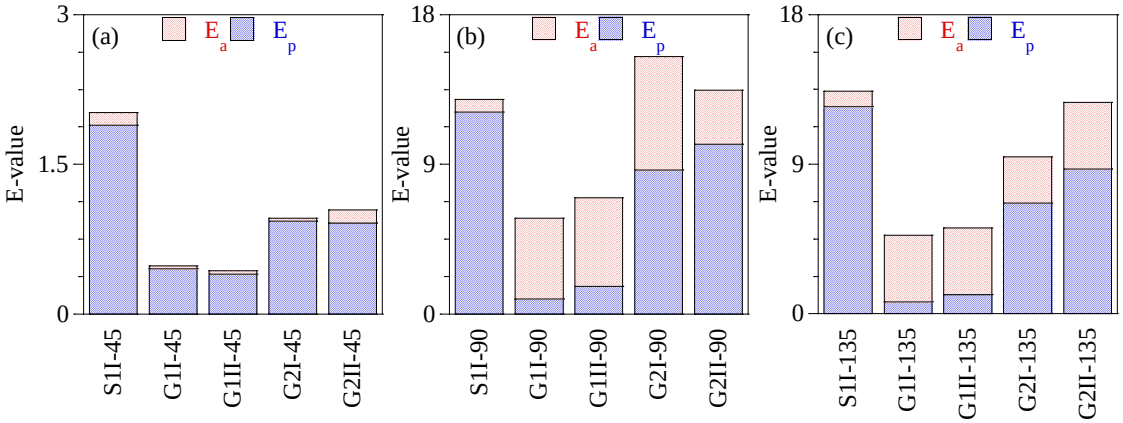

FIGURE 29 – Absorbed Energy (a) 45°; (b) 90°; (c) 135°

Similarly, FIGURE 29 shows the total absorbed energy, E_T as the sum of E_a and E_p for each push-off specimen. Overall, the GFRP, 45-degree specimens (see FIGURE 29(a)) show lower concrete contributions when compared to other orientation angles (see FIGURE 29(b) and (c)). On average, the GFRP, 90-degree specimens (see FIGURE 29(b)) had larger E_T values. The GFRP reinforcement exhibited more slip resulting in the increase of aggregate interlock. The slightly lower E_T values of the 135-degree specimens indicates brittle behavior and abrupt failure after the peak shear force.

The two-bar specimens exhibited larger E-values when compared to the one-bar specimens. The additional reinforcement provides additional confinement resulting in increased concrete contributions. To achieve larger and equal contributions of concrete before and after the peak, the reinforcement should have some degree of ductility but enough stiffness to resist abrupt failure.

F. Summary of Test Results

The orientation angle significantly affected the shear capacity of the push-off specimens containing one reinforcing bar. In all orientations, GFRP and steel reinforcement had similar shear capacities. Reinforcement orientations of 45-degrees, showed an inferior ability to resist displacement of the crack width and slip before reaching an adequate tensile capacity (both GFRP and steel). The 90 and 135-degree orientations allowed both reinforcements (i.e., GFRP and steel) to reach similar strengths to what was found by tension tests, regardless of aggregate interlock. This indicates near full performance of the reinforcement, and is a favorable condition when designing a reinforced concrete element.

Similarly, the orientation angle significantly affected the shear capacity of push-off specimens containing two reinforcing bar. Shear capacities increased with the addition of another GFRP bar. In 90-degree specimens, the observation of longitudinal splitting cracks forming around the reinforcement caused bond degradation between the reinforcement and concrete, which could have caused a loss in shear capacity. However, the second bar provided additional capacity with respect to shear capacity. On average, the GFRP, 90-degree specimens had larger E_T values, while the 135-degree specimens had lower E_T values, indicating brittle behavior and abrupt failure after the peak shear force.

V. CONCLUSIONS AND RECOMMENDATIONS

A. Conclusions

Fifteen push-off tests were conducted to characterize the shear behavior of GFRP reinforcement embedded in concrete. The mechanical properties of the steel and GFRP were determined to confirm the strengths of the materials. The following conclusions were drawn as follows:

1. Tensile strength and elastic modulus of steel, Grades 60 and 80, and GFRP reinforcement were determined. GFRP reinforcement exhibited a higher tensile strength but lower modulus of elasticity when compared with the equivalent size of steel reinforcement.
2. The steel reinforced push-off specimens exhibited higher peak shear strengths compared to the equivalent GFRP reinforcement. However, the pre and post-peak behavior of steel and GFRP reinforcement is distinctively different. Pre-peak behavior of the steel reinforced specimens exhibited lower crack width up to the peak shear force. Conversely, the GFRP reinforced specimens exhibited more crack width and slip at peak shear force. After the peak, GFRP reinforced specimens did not have sufficient sustained load, indicating brittleness.
3. Specimens with a single GFRP reinforcing bar exhibited three distinct failure modes (Mode I, Mode II, and Mixed Mode) with respect to the bar's orientation. Compressive and tensile failures characterized Modes I and Mode II, respectively. The Mixed mode exhibited both compressive and tensile failure of the bars. Specimens reinforced with two GFRP bars exhibited

similar failure modes as specimens reinforced with one-bar. A group-effect was observed along with the propagation of longitudinal splitting cracks. However, the shear capacity of the two-bar system is approximately two times greater than the one-bar system. These cracks caused bond failure in one of the reinforcing a bars prior to peak failure, resulting in losses of shear capacity and termination of testing.

4. It is concluded that based on the orientation, GFRP and steel reinforcement exhibit significantly different behavior. The 135-degree orientation was determined to produce the most desirable conditions for all reinforcement bars. This orientation allowed the GFRP reinforcement to reach similar strength to that found during tension tests, regardless of any aggregate interlock. To quantify this, the two stages of energy absorption (i.e., E-values) are introduced. This orientation also affected the energy absorption capacities provided by the reinforcement and aggregate interlock. Higher confinement properties were exhibited in the 90 and 135-degree orientation with similar E-values.

B. Recommendations

From the previous conclusions stated, the change of crack angles in beams will lead to changes in the bar orientation with respect to the crack plane. Therefore, the contribution of reinforcement to shear capacity can be significantly varied depending on the crack angle. This was found in this study. In the future, the design code can be further calibrated to implement this concept to improve the integrity and reliability of the design equations. For

safe and conservative design, the limit strains currently in use must also be re-evaluated and tested with further research.

The long-term performance and durability of GFRP is also another area for future research, along with the bond performance between GFRP and concrete.

REFERENCES CITED

AASHTO. 2009. *LRFD Bridge Design Specifications.* Washington, D.C.:American Association of Highway and Transportation Officials (AASHTO).

ACI 211.1. 1991. *Standard practice for selecting proportions for normal, heavyweight, and mass concrete: procedure for mix design*. Farmington Hills, MI. American Concrete Institute (ACI). 38.

ACI 318. 2011. *Building code requirements for structural concrete and commentary*. Farmington Hills, MI. American Concrete Institute (ACI). 503.

ACI 440. 2006. *Guide for the design construction of concrete reinforced with FRP bars*. Farmington Hills, MI. American Concrete Institute (ACI). 44.

ACI 445. 1998. Recent approaches to shear design of structural concrete. *Journal of Structural Engineering.* 124: 1375-1417.

Alam, M. S., and Hussein, A. 2012. Effect of Member Depth on Shear Strength of High-Strength Fiber-Reinforced Polymer–Reinforced Concrete Beams. *Journal of Composites for Construction.* 16: 119-126.

Ali, M., Oehlers, D., and Griffith, M. 2008. Shear transfer across cracks in FRP strengthened RC members. *ASCE Journal of Composite Construction.* 12: 416-424.

Ametrano, D. (2011). "Bond characteristics of glass fibre reinforced polymer bars embedded in high performance and ultra-high performance concrete." Ryerson University.

ASCE. "Report Card for America's Infrastructure." http://www.infrastructurereportcard.org/a/#p/bridges/overview. 7 April 2013

ASTM A370. 2013. *Standard Test Methods and Definitions for Mechanical Testing of Steel Products*. West Conshohocken, PA. ASTM International.

ASTM A615. 2014. *Standard Specification for Deformed and Plain Carbon-Steel Bars for Concrete Reinforcement*. West Conshohocken, PA. ASTM International.

ASTM C33. 2013. *Standard Specifications for Concrete Aggregates*. West Conshohocken, PA. ASTM International.

ASTM C39. 2014. *Standard Test Method for Compressive Strength of Cylindrical Concrete Specimens*. West Conshohocken, PA. ASTM International.

ASTM C127. 2013. *Standard Test Method for Density, Relative Density (Specific Gravity), and Absorption of Coarse Aggregate*. West Conshohocken, PA. ASTM International.

ASTM C136. 2013. *Standard Test Method for Sieve Analysis of Fine and Coarse Aggregates*. West Conshohocken, PA. ASTM International.

ASTM C143. 2012. *Standard Test Method for Slump of Hydraulic-Cement Concrete*. West Conshohocken, PA. ASTM International.

ASTM C192. 2012. *Standard Practice for Making and Curing Concrete Test Specimens in the Laboratory*. West Conshohocken, PA. ASTM International.

ASTM C496. 2011. *Standard Test Method for Splitting Tensile Strength of Cylindrical Concrete Specimens*. West Conshohocken, PA. ASTM International.

ASTM C566. 2013. *Standard Test Method for Total Evaporable Moisture Content of Aggregate by Drying*. West Conshohocken, PA. ASTM International.

ASTM D7205. 2011. *Standard Test Method for Tensile Properties of Fiber Reinforced Polymer Matrix Composite Bars* West Conshohocken, PA. ASTM International.

Bentz, E., Vecchio, F., and Collins, M. 2006. Simplified modified compression field theory for calculating shear strength of reinforced concrete elements. *ACI Structural Journal.* 103: 614-624.

Birkeland, P., and Birkeland, H. 1966. Connections in precast concrete construction. *ACI Journal.* 63: 345-368.

CNR. CNR-DT-203/2006. 2006. *Guide for the design and construction of concrete structures reinforced with fiber-reinforced polymer bars*. Rome. Advisory Committee on Technical Recommendations for Construction. 39.

CSA. CAN/CSA-S6-06. 2006. *Canadian highway bridge design code*. Rexdale. Canadian Standards Association (CSA). 733.

CSA. CSA S806-12. 2012. *Design and construction of building components with fiber-reinforced polymers*. Toronto. Canadian Standards Association (CSA).

Dally, J., and Riley, W. 1991. *Experimental stress analysis.* New York:McGraw Hill.

El-Sayed, A., El-Salakawy, E., and Benmokrane, B. 2005. Shear strength of one-way concrete slabs reinforced with fiber-reinforced polymer composite bars. *Journal of Composites for Construction.* 9: 147-157.

FHWA. "Current Practices in FRP Composites Technology." https://www.fhwa.dot.gov/bridge/frp/deckprac.cfm. 6 May 2014

Gardoni, P., Trejo, D., and Kim, Y. H. 2012. Time-Variant Reliability Analysis and Flexural Design of GFRP-Reinforced Bridge Decks. *Journal of Composites for Construction.* 16: 359-370.

Hoult, N., Sherwood, E., Bentz, E., and Collins, M. 2008. Does the use of FRP reinforcement change the one-way shear behavior of reinforced concrete slabs. *Journal of Composite Construction.* 12: 125-133.

JSCE. Concrete engineering series no. 23. 1997. *Recommendation for design and construction of concrete structures using continuous fiber reinforcing materials*. Tokyo. Japan Society of Civil Engineers (JSCE).

Kara, I. F. 2011. Prediction of shear strength of FRP-reinforced concrete beams without stirrups based on genetic programming. *Advances in Engineering Software.* 42: 295-304.

Keller, T. 2001. Recent all-composite and hybrid fibre-reinforced polymer bridges and buildings. *Progress in Structural Engineering and Materials.* 3: 132-140.

Kim, Y. H., Hueste, M. B. D., Trejo, D., and Cline, D. B. H. 2010. Shear Characteristics and Design for High-Strength Self-Consolidating Concrete. *Journal of Structural Engineering.* 136: 989-1000.

Machial, R., Alam, M. S., and Rteil, A. 2012. Revisiting the shear design equations for concrete beams reinforced with FRP rebar and stirrup. *Materials and Structures.* 45: 1593-1612.

Mansur, M., Vinayagam, T., and Tan, K. 2008. Shear transfer across a crack in reinforced high-strength concrete. *Journal of Materials in Civil Engineering.* 20: 214-217.

Martín-Pérez, B., and Pantazopoulou, S. J. 2001. Effect of bond, aggregate interlock and dowel action on the shear strength degradation of reinforced concrete. *Engineering Structures.* 23: 214-227.

Mast, R. 1968. Auxillary reinforcement in concrete connections. *ASCE Structural Journal.* 94: 1485-1504.

Mattock, A. 1974. Shear transfer in concrete having reinforcement at an angle to the shear plane. *ACI Special Publication.* 42: 14-42.

Park, R., and Paulay, T. 1975. *Reinforced Concrete Structures.* New York:

Rahal, K. 2010 Shear-transfer strength of reinforced concrete. *ACI Structural Journal.* 107: 419-426.

Razaqpur, A., Shedid, M., and Isgor, B. 2011. Shear strength of fiber-reinforced polymer reinforced concrete beams subject to unsymmetric loading. *Journal of Composite Construction.* 500-512.

Razaqpur, A., and Spadea, S. 2014. Shear strength of FRP reinforced Concrete Members with stirrups. *Journal of Composites for Construction.* 15: 1-15.

Santos, P., Julio, E., and Santos, J. 2010. Towards the development of an in situ non-destructive method to control the quality of concrete-to-concrete interfaces. *Engineering Structures.* 32: 207-217.

Tureyen, A. K., and Frosh, R. J. 2003. Concrete shear strength: another perspective. *ACI Structural Journal.* 100: 609-615.

Vecchio, F., and Collins, M. 1986. The modified compression field theory for reinforced concrete elements subjected to shear. *Journal of American Concrete Institute.* 83: 219-231.

Walraven, J. 1981. Fundamental analysis of aggregate interlock. *Journal of Structural Division-ASCE.* 107: 2245-2270.

Wegian, F., and Abdalla, H. 2005. Shear capacity of concrete beams reinforced with fiber reinforced polymers. *Composite Structures.* 71: 130-138.

Wight, J., and MacGregor, J. 2012. *Reinforced Concrete: Mechanics and Design.* Upper Saddle River, NJ:Pearson Education, Inc.

APPENDIX I

1. Concrete Strength Data

Compressive Test				Splitting Tensile			
	Load	Strength	Average		Load	Strength	Average
G1A-45	88500	7041	7285	G1A-45	-	-	-
	94500	7518			-	-	
	91700	7295			-	-	
G1B-45	85900	6834	6908	G1B-45	30500	607	607
	88100	7009			29500	587	
	86500	6881			31500	627	
G2C-45	88500	7041	7062	G2C-45	36300	722	706
	87700	6977			33700	670	
	90100	7168			36500	726	
G2D-45	91500	7279	7263	G2D-45	35900	714	718
	90900	7232			36500	726	
	91500	7279			35900	714	
S1E-45	81300	6468	6431	S1E-45	30900	615	592
	77500	6165			31900	635	
	83700	6659			26500	527	
G1A-90	90500	7200	7152	G1A-90	37300	742	696
	88900	7072			35900	714	
	90300	7184			31700	631	
G1B-90	85300	6786	6834	G1B-90	33300	662	643
	84900	6754			30500	607	
	87500	6961			33100	659	
G2C-90	83500	6643	6728	G2C-90	35700	710	706
	84700	6738			35500	706	
	85500	6802			35300	702	
G2D-90	83900	6675	6680	G2D-90	35100	698	712
	84100	6691			35700	710	
	83900	6675			36500	726	
S1E-90	77100	6134	6431	S1E-90	26700	531	576
	84300	6706			29500	587	
	81100	6452			30700	611	
G1A-135	91300	7263	7232	G1A-135	27900	555	613
	90100	7168			31500	627	
	91300	7263			33100	659	
G1B-135	83300	6627	6685	G1B-135	29100	579	655

	83100	6611			33500	666	
	85700	6818			36100	718	
	95900	7629			29100	579	
G2C-135	96300	7661	7624	G2C-135	35900	714	645
	95300	7582			32300	643	
	83500	6643			32500	647	
G2D-135	86700	6897	6855	G2D-135	34700	690	659
	88300	7025			32100	639	
	80300	6388			32100	639	
S1E-135	79300	6309	6436	S1E-135	31700	631	639
	83100	6611			32500	647	
Average		6866		Average		642	
St. Dev		371		St. Dev		45	

2. Steel Tension Test Data

Rebar Size	1/2"	Ultimate Stress, psi	104253
Grade, ksi	80	Ultimate Strain, in/in	0.1150
Initial Total Length, in	8	Modulus of Elasticity	30.33E+6
Initial Gage Length, in	3.018	Modulus of Toughness	911751
Average Diameter, in	0.455	Proportional Limit	2486 ue, 67164 psi
Crossectional Area, in^2	0.20	Percent Elongation, %	11.50
Final Total Length, in	8.347	Yield Strain, ue	5177
Final Gage Length, in	3.365	Yield Stress, psi	89717
Max Force, P, lb	20470		

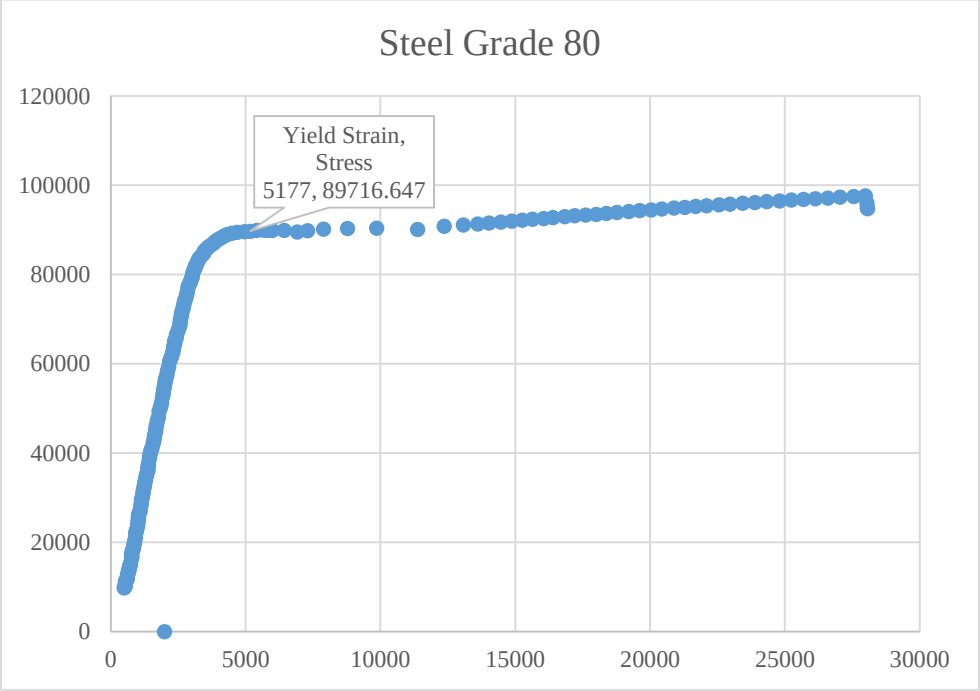

Rebar Size	1/2"	Ultimate Stress, psi	109550
Grade, ksi	60	Ultimate Strain, in/in	0.1576
Initial Total Length, in	7	Modulus of Elasticity	32.16E+6
Initial Gage Length, in	3.020	Modulus of Toughness	409269
Average Diameter, in	0.457	Proportional Limit	2086 ue, 59493 psi
Crossectional Area, in^2	0.20	Percent Elongation, %	15.76
Final Total Length, in	7.476	Yield Strain, ue	2413
Final Gage Length, in	3.496	Yield Stress, psi	65313
Max Force, P, lb	21510		

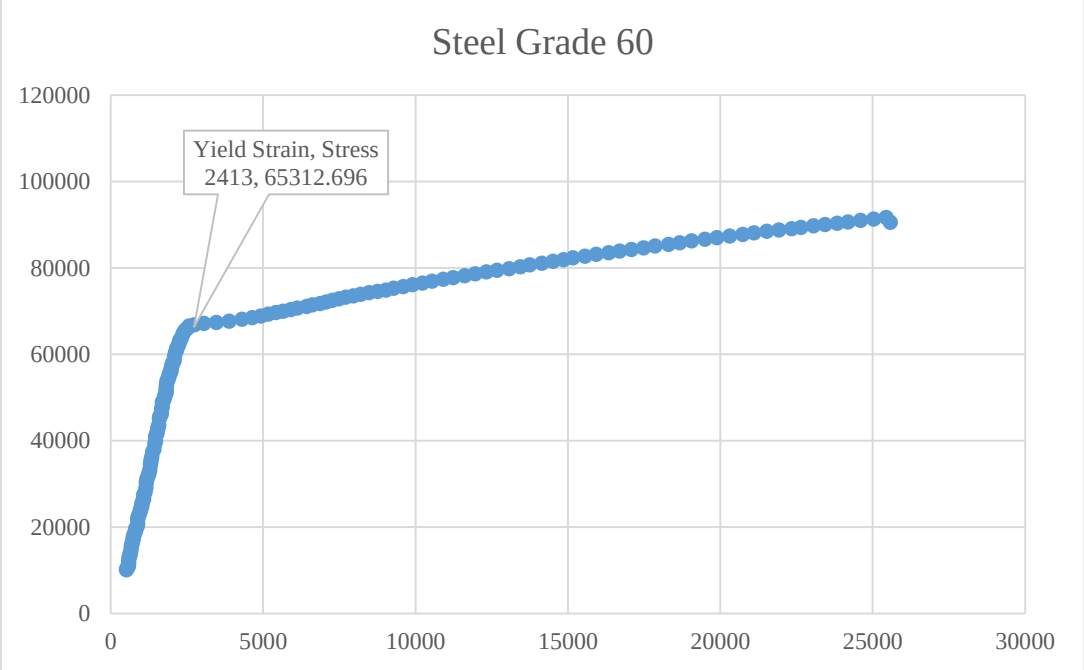

Rebar Size	1/2"	Ultimate Stress, psi	106341
Grade, ksi	60	Ultimate Strain, in/in	0.1735
Initial Total Length, in	8	Modulus of Elasticity	25.35E+6
Initial Gage Length, in	3.015	Modulus of Toughness	2135801
Average Diameter, in	0.454	Proportional Limit	2296 ue, 62754 psi
Crossectional Area, in^2	0.20	Percent Elongation, %	17.35
Final Total Length, in	8.523	Yield Strain, ue	4869
Final Gage Length, in	3.538	Yield Stress, psi	67223
Max Force, P, lb	20880		

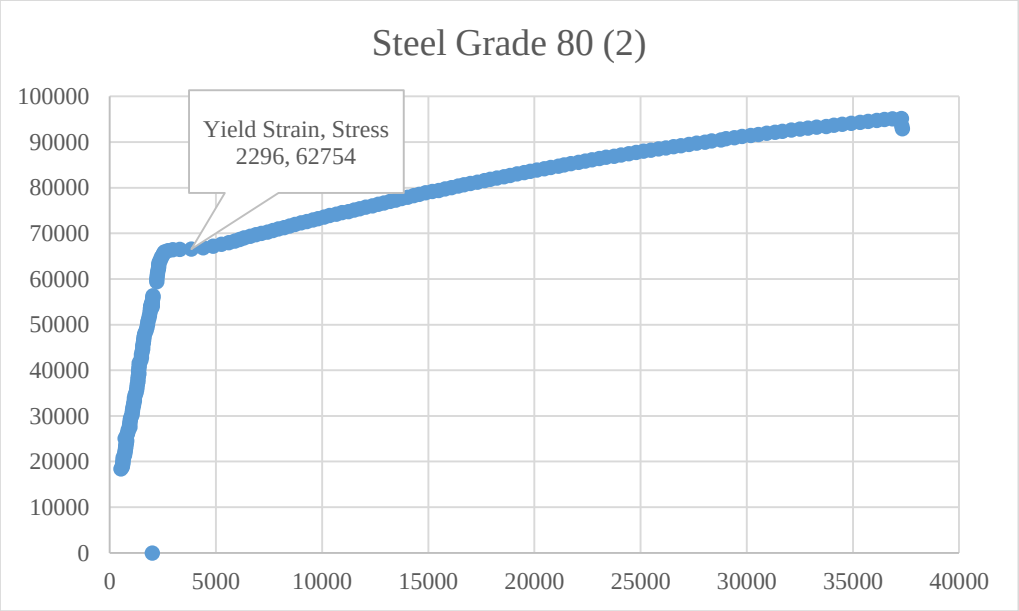

3. GFRP Tension Test Data

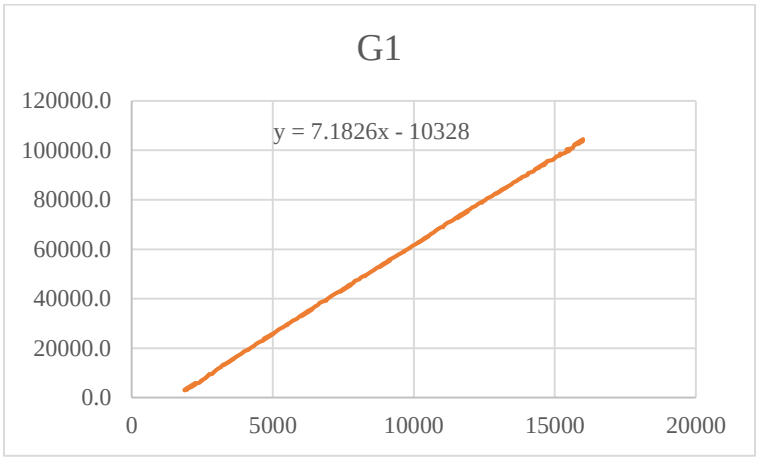

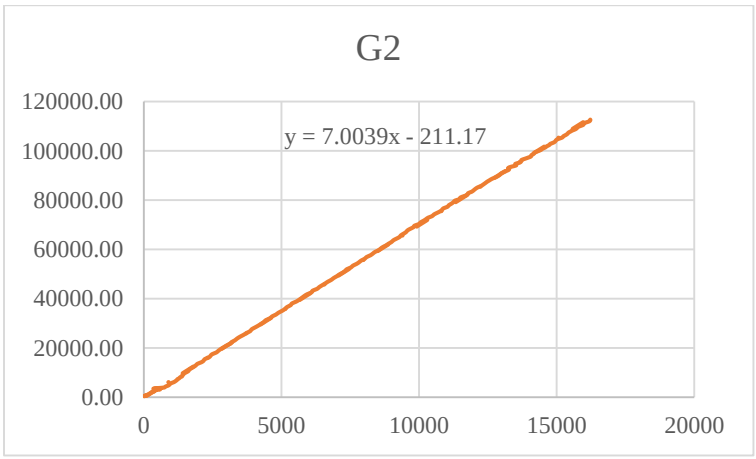

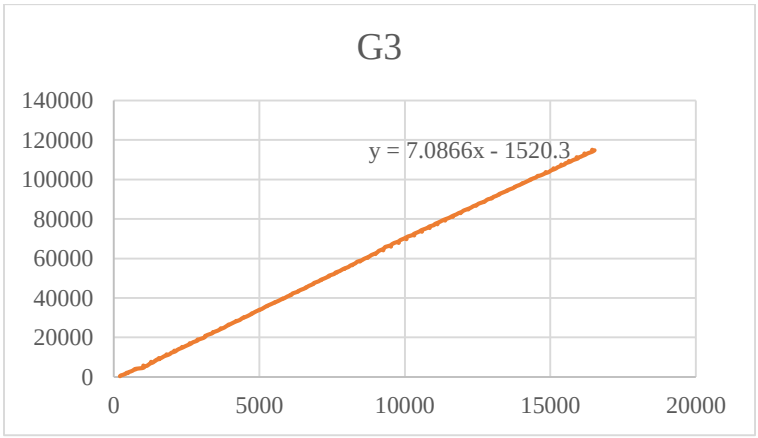

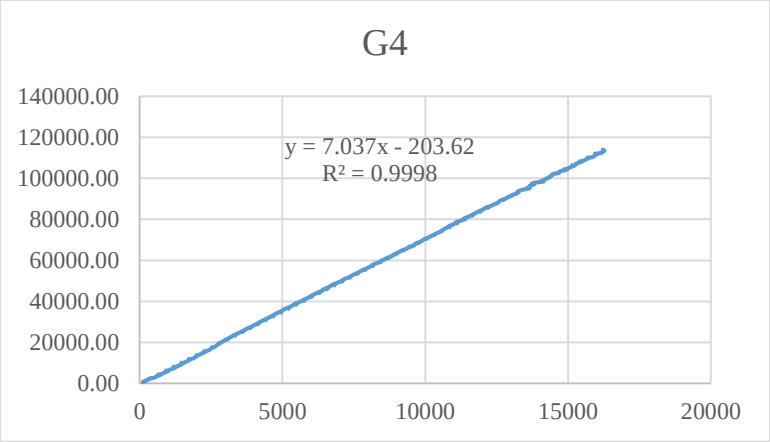

4. Notation

A_f = area of frp reinforcement

A_{fv} = area of frp reinforcement within spacing, s

A_v = area of frp reinforcement

$A_{v,\min}$ = minimum area of frp reinforcement needed to prevent failure of flexural members

a = shear span

a_g = area of aggregates

b = width of beam

b_w = width of web

C = spacing or cover dimension

CA = coarse aggregate

$c_0 = 7.696$

$c_1 = 7.254$

$c_2 = 7.718$

c = distance from extreme compression fiber to neutral axis

d = diameter of cylinder

d = distance from extreme compression fiber to centroid of tension reinforcement

d_b = diameter of reinforcing bar

d_v = shear depth

E = modulus of elasticity

E_a = absorbed energy pre-peak

E_c = modulus of elasticity of concrete

E_f = modulus of elasticity of frp

E_{fl} = modulus of elasticity of longitudinal frp

E_{fv} = modulus of elasticity of frp

E_p = absorbed energy post-peak

E_s = modulus of elasticity of steel

E_T = total absorbed energy

FA = fine aggregate

$f_c^{'}$ = compressive strength of concrete

$f_{mcd}^{'}$ = design compressive strength of concrete

f_{cr} = cracking strength of concrete

$f_{ctk\,0.05}$ = characteristic concrete tensile strength

f_{fb} = strength of bent portion of frp bar

f_{fd} = design tensile strength of GFRP bars considering environmental reduction factors

f_{fr} = required bar stress

$f_{frpbend}$ = strength of bent portion of frp bar

f_{fu} = design tensile strength of frp

f_{fv} = tensile strength of frp for shear design

f_t = tensile strength of concrete

f_u = ultimate tensile strength of frp

f_v = shear strength of frp

$f_{vcd} = 0.23\sqrt[3]{f_{cd}^{'}}$, provided that $f_{vcd} \leq 0.72$

f_y = specified yeild strength of steel

h = overall height of flexural member

$jd = d / 1.15$

k = ratio of depth of neutral axis to reinforcement depth

k_a = enhancement of shear resistance by arch effect

k_d = enhancement of shear resistance by dowel effect

k_m = moment to shear ratio

k_r = longitudinal reinforcement rigidity

k_s = account for size effect

l = length of flexural memebr

M_d = design bending moment

M_f = factored moment at a section

M_o = bending moment required to cancel out axial force stresses

n_f = ratio of modulus of elasticity of frp bars to modulus of elasticity of concrete

P = maximum applied force

R = support reaction

r_b = internal radius of bend in frp reinforcement

s = stirrup spacing or pitch of continuous spirals and longitudinal frp bar spacing

s_{ze} = equivalent crack spacing parameter

T = tensile force

V = shear force

V_a = total shear force due to arch action

V_{ax} = x-component of shear force due to arch action

V_{ay} = y-component of shear force due to arch action

V_c = nominal shear strength provided by concrete

V_d = nominal shear strength provided by dowel action

V_{frp} = shear strength of frp

V_f = nominal shear strength provided by frp reinforcement

V_{fv} = shear strength of frp stirrups

V_n = total nominal shear capacity of flexural member

V_{peak} = peak shear force

$V_{Rd,c}$ = nominal shear strength of concrete

$V_{Rd,ct}$ = nominal shear strength of concrete

V_r = factored shear resistance

V_s = nominal shear strength provided by reinforcement

V_{sF} = nominal shear strength provided by frp reinforcement

α_s = angle formed by shear reinforcement and member axis

β = ratio of distance from neutral axis to extreme tension fiber to distance from neutral axis to center of tensile reinforcement

β_d = reduction factor used for deflection calculation

$$\beta_n = 1 + \frac{M_o}{M_d} \le 2 \text{for} N_f \ge 0 \text{ or } 1 + \frac{2M_o}{M_d} \le 2 \text{for} N_f < 0$$

$$\beta_p = \left(100 \frac{\rho_{fl} E_{fl}}{E_s} \right)^{\frac{1}{3}} \le 1.5$$

δ_{cs} = crack slip displacement

$\delta_{cs,final}$ = final crack slip displacement

$\delta_{cs,peak}$ = peak crack slip displacement

δ_{cw} = crack width displacement

ε_1 = longitudinal mid-depth strain at shear failure

ε_{fv} = rupture strain of frp

ε_u = ultimate strain of steel

ε_x = longitudinal strain at midheight of the cross section

ε_y = yield strain of steel

ϕ_c = material resistance factor

$\varphi_c = 0.75$

φ_f = 0.5 for GFRP and 0.75 for CFRP

$\gamma_b = 1.15$

$\gamma_d = 1.3$

$\gamma_f = 1.5$

$\gamma_{f,\varphi} = 2$

λ = concrete density factor

$\mu\varepsilon$ = micro-strain

π = value of pi

θ = angle of inclination of frp stirrups

ρ_f = frp reinforcement ratio

ρ_{fl} = longitudinal frp reinforcement ratio

ρ_{fv} = frp shear reinforcement ratio

σ = normal stress

σ_{fv} = vertical stress in frp stirrup

σ_n = stress in concrete due to axial loads

$\tau_{Rd} = 0.25 f_{ctk,0.05}$

$\upsilon = 0.7 - f_c / 200 \geq 0.5$

VITA

Mr. Austin Connor received a Bachelor's of Science in Civil Engineering in the summer of 2013 from the University of Louisville, Louisville, Kentucky. As an undergraduate, Austin was the recipient the Woodford R. Porter scholarship and Undergraduate Research Scholarship from the Commission on Diversity and Racial Equality. Previously, he worked at the U.S. Army Corps of Engineers, Louisville District from January 2011 to May 2013 as a student engineer. He is currently a Master's of engineering graduate student and is expected to graduate in the summer of 2014. He is a graduate research and teaching assistant in the Civil and Environmental Engineering department. He is currently conducting research to investigate the shear properties of Glass-Fiber-Reinforced Polymer reinforcement in concrete systems. The Multimodal Transportation and Infrastructure Consortium (MTIC) selected Austin as the Transportation Research Board Outstanding Student of the Year for 2014. His focus area is to develop the design methodology using innovative construction materials for sustainable development of transportation infrastructure systems. After graduation, he is expected to pursue a Ph.D. at the University of Louisville. Austin was a recipient of a fellowship from the Southern Regional Education Board (SREB) – KY State Doctoral Scholar Program. He is an active member in several on-campus organizations such as, Triangle Fraternity (Alumnus), the ASCE student chapter, the Society of Porter Scholars, and the Civil Engineering Honor Society, Chi Epsilon.